Engineered, Perfusable, Human Microvascular Networks on a Microfluidic Chip

by

Jordan Ari Whisler

B.S. Mechanical Engineering
Washington University in St. Louis, 2009

SUBMITTED TO THE DEPARTMENT OF MECHANICAL ENGINEERING IN PARTIAL FULFILLMENT OF THE REQUIREMENTS FOR THE DEGREE OF

MASTER OF SCIENCE IN MECHANICAL ENGINEERING

AT THE

MASSACHUSETTS INSTITUTE OF TECHNOLOGY

SEPTEMBER 2013

Signature of Author: _____

Department of Mechanical Engineering

August 26, 2013

Certified by: _____

Roger D. Kamm

Professor of Mechanical Engineering

Thesis Supervisor

Accepted by: _____

David E. Hardt

Chairman, Committee for Graduate Students

Department of Mechanical Engineering

Engineered, Perfusable, Human Microvascular Networks on a Microfluidic Chip

by

Jordan Ari Whisler

Submitted to the Department of Mechanical Engineering on August 26, 2013 in Partial Fulfillment of the Requirements for the Degree of

Master of Science in Mechanical Engineering

ABSTRACT

In this thesis, we developed a reliable platform for engineering perfusable, microvascular networks on-demand using state of the art microfluidics technology. We have demonstrated the utility of this platform for studying cancer metastasis and as a test bed for drug discovery and analysis. In parallel, this platform enabled us to study, in a highly controlled environment, the physiologic processes of angiogenesis and vasculogenesis to further elucidate their underlying mechanisms.

In addition to using our platform for real-time observation of physiological processes, we also took advantage of the ability to influence these processes through precise control of the extracellular environment. By manipulating the mechanical and bio-chemical inputs to our system, we controlled the dynamics of microvascular network formation as well as key properties of the network morphology. These findings will aid in the design and engineering of organ specific constructs for tissue engineering and regenerative medicine applications.

Finally, we explored the potential use of stem cells for engineering microvascular networks in our system. We found that human mesenchymal stem cells can act as secondary, support cells during microvascular network formation.

Thesis Supervisor: Roger D. Kamm

Title: Cecil and Ida Green Distinguished Professor of Biological and Mechanical Engineering

Acknowledgments

I would like to thank my advisor, Professor Roger Kamm, for his scientific insight as well as his motivation and support throughout this project. He was willing to take me in as an inexperienced researcher with little background in biology, and had the foresight and patience to allow me to develop the necessary skills to complete a successful project and make an independent contribution to the scientific community. His rigorous scientific and ethical standards serve as an example for all of his students.

A special thanks to Joan and Leslie, in the MechE grad office, for keeping me up to date with all the requirements and deadlines and making sure that this thesis became a reality. You are always looking out for your students, and we greatly appreciate it.

I would also like to thank my parents for their continuous support throughout my academic career thus far. They have always encouraged me to pursue my passions and provided me the resources to do so. They have instilled in me the belief that any accomplishment is possible with the right attitude and lots of hard work.

Finally, I would like to thank my fiancée, Rena. You have experienced my late nights in the lab and intensely focused periods of writing, and you still want to marry me. In truth, the long hours are bearable only because I know you will be there waiting when I finish.

The material in this thesis is based upon work supported by the National Science Foundation Graduate Research Fellowship and the Science and Technology Center Emergent Behaviors of Integrated Cellular Systems (EBICS) Grant No. CBET-0939511.

Table of Contents

Introduction 7

Chapter 2: Microfluidic Device Fabrication and Designs 9

Device Design 9

Device Fabrication 10

Gel Filling Method 10

Micro-injection 10

Gel Filling Port 11

Comparison 12

Chapter 3: Vascularization Strategies 14

Angiogenesis 14

Seeding 15

Angiogenesis Device 15

Results 17

Alginate Beads 18

Bead Forming Methods 19

Results and Discussion 22

Intermediate Post Device 23

Vasculogenesis 25

Comparison 27

Chapter 4: Control of Microvascular Network Morphology 29

Angiogenesis 30

Effects of Extracellular Matrix 30

Growth factors 34

Interstitial flow 35

Vasculogenesis 38

Materials and Methods 40

Results 43

Discussion 50
Chapter 5: Stem Cells for Microvascular Engineering 55
Human Mesenchymal Stem Cells (hMSCs) 55
Mouse Embryonic Stem Cells (mESCs) 57
Conclusion and Future Directions 60
References 61
Appendix I: Seeding ECs in Fibrin Gel 65
Appendix II: P-Values for Figures 17-20 66

List of Figures

Figure 1. Two designs implementing the gel filling port system.. 12
Figure 2. Diagram and results using angiogenesis gel filling device. 17
Figure 3. Confocal images of perfusable microvascular network formed using angiogenisis method.. ... 18
Figure 4. Schematic diagram of the air-cutting method for producing alginate beads..... 20
Figure 5. Setup of the two-phase microfluidic alginate bead making system.. 21
Figure 6. Alginate bead angiogenesis device. 22
Figure 7. Dextran permeability experiments. 23
Figure 8. Intermediate post device. 24
Figure 9. Results from intermediate post device. 25
Figure 10. Vasculogenesis experiments. 26
Figure 11. ECM composition comparison. 31
Figure 12. PEG gel immobilization of fibroblasts. 32
Figure 13. Mechanical effects on angiogenesis. 33
Figure 14. Biochemical effects on angiogenesis. 34
Figure 15. Interstitial flow effects on angiogenesis. 36
Figure 16. Multiculture vasculogenesis device: diagram and results. 39
Figure 17. Fibroblast stabilization. 44
Figure 18. Paracrine siganling effects on vasculogenesis network morphology. 46
Figure 19. Fibrin concentration effects on vasculogenesis network morphology. 47
Figure 20. EC seeding density effects on vasculogenesis network morphology. 49
Figure 21. Control of microvascular network morphology: aproach and results. 53
Figure 22. Human bone marrow derived MSCs cultured with ECs in our microfluidic device.. 56
Figure 23. Mouse embryonic stem cells for angiogenesis. 57
Figure 24. Mouse embryonic stem cells for vasculogenesis. 58

Introduction

These are exciting times for the fields of Tissue Engineering and Regenerative Medicine. Recent headlines have reported the successful implantation of engineered tracheas, bladders, and urethras in human patients.[1–3] There are currently several viable products on the market for cell-based skin grafts used to treat burn and wound victims.[4,5] All these tissues can be grown from a patient's own cells, reducing the risk of rejection by the body.

To date, however, the success stories have been limited to thin tissues providing basic structural function which do not require a functional vasculature for tissue survival. In order to engineer sustainable thick and complex tissues and organs, it will be necessary to include such vasculature to provide oxygen and nutrients to the cells to meet their metabolic needs upon implantation.[6] This is the goal of microvascular tissue engineering.

Tissue engineers are currently pursuing two approaches to supplying engineered tissues with a functioning microvasculature: 1) host induced vascularization and 2) pre-vascularization. The former attempts to minimize the time that implanted cells must survive without a proper nutrient supply by inducing angiogenesis from the host vasculature through a combination of angiogenesis promoting matrix ligands and growth factor delivery.[7] The latter attempts to eliminate the time to vascularization by engineering a functional vasculature into the tissue construct before implantation.[8,9] Successful implementation will likely comprise a combination of the two. The findings of our work advance the causes of both approaches. Our pre-vascularized tissue constructs can potentially be implanted directly into the body for therapeutic applications. Additionally, the platform has enabled us to study the process of

vascularization in great detail, providing insight and strategies for more quickly and effectively inducing angiogenesis in-vivo.

In this thesis, we present the development and application of a new microfluidic platform for engineering perfusable microvascular networks in a 3D environment.

Chapter 2 discusses the technical designs and methods for fabrication of the device and carrying out cell culture experiments.

Chapter 3 describes the various forms of vascularization that our device is capable of replicating along with a discussion of the relevant applications for each.

Chapter 4 presents our major contribution to the field of microvascular tissue engineering in our efforts to control the process of vascularization using the mechanical and biochemical inputs of our microfluidic system.

Chapter 5 describes our studies on the use of stem cells for microvascular tissue engineering and cell therapies.

Chapter 2: Microfluidic Device Fabrication and Designs

To carry out our work, we have taken advantage of the latest in microfluidic technology for mammalian cell-culture. The use of microfluidics for cell culture provides several advantages over traditional biological assays.[10] The miniaturization of in-vitro lab experiments through the use of microfluidics enables many conditions to be tested while minimizing the volume of expensive reagents used. It allows for precise control of the geometry and the chemical composition of the environment in which cells are cultured. Importantly for our studies, it allows for spatial segregation of cell types while still maintaining close enough proximity for the cells to communicate. It also enables controlled fluid flow to be applied to cells cultured in 3D.

Device Design

We based the design of our microfluidic device for vascularization upon previous designs from our lab for devices used to study the initial stages of sprouting angiogenesis.[11–13] These designs provide a vertical interface between the hydrogel and the medium channel (see Figures 1 & 2 for illustrative diagrams) on which a confluent endothelial monolayer can be formed. It is from this vertical monolayer that the endothelial cells sprout horizontally in to the hydrogel, enabling the process to be visualized in real time using standard microscopy. We needed to make several key adjustments to these previous designs to ensure complete, efficient, and uniform vascularization of the entire gel region. These adjustments, and the findings that motivated them, are further discussed in Chapter 3.

Device Fabrication

We used standard procedure for generating silicone molds.[14] Briefly, CAD designs were generated and used to print negative pattern transparency masks. A 100 μm layer of SU-8 photoresist was coated onto a silicon wafer, and the mask was used to photo-polymerize the pattern on to the wafer.

The mask was repeatedly used to form microfluidic chips. Briefly, PDMS (Ellsworth Adhesives, WI USA) and curing agent were mixed at a 10:1 ratio and poured onto the wafer. After degassing, the PDMS was baked in an 80 degree oven for two hours. The individual devices were then cut out and a biopsy punch was used to create ports for gel filling and medium channels. Tape was used to remove dust from the surface, and the devices were placed in an autoclave for sterilization. Clean devices and coverslips were plasma treated (Harrick Plasma, CA, USA) and bonded together.

Gel Filling Method

We used two different techniques for filling the gel chamber of our microfluidic device with hydrogel: **(1)** micro-injection **(2)** and gel-filling via a port in the closed device. Each technique presents its own advantages and disadvantages. Ultimately, the gel-filling design was preferred due to its consistent formation of a uniform gel/channel interface and avoidance of leakage.

Micro-injection

In the micro-injection method developed by Vickerman et. al.[15] (see this reference for a detailed protocol and parts list), sterile devices are plasma treated and allowed to recover some

hydrophobicity before the gel is inserted manually into the gel cage. This timing is critical since the surfaces must be sufficiently hydrophobic to ensure irreversible bonding of the device to the glass coverslip after the gel is filled. However, if the PDMS surface is too hydrophobic, the gel will leak out into the medium channels during filling. We determined empirically that the window of opportunity lies within 30-60 min after plasma treatment. The exact time is variable and can depend on the inconsistent performance of the plasma etching machine. To fill the gel, a liquid phase mixture of the hydrogel is prepared over ice in an eppendorf tube. 2-4 µl of this mixture is collected in a pipette and filled by hand or by using the microinjection setup as described by Vickerman et. al.[15] The coverslip is then immediately bonded to the PDMS and pressed evenly to form a good seal.

Gel Filling Port

The major difference in the gel filling port design is that the gel is filled after the coverslip has already been bonded to the PDMS device. In this system, the bonded device should be allowed to sit for 24 h after plasma treatment in order to recover hydrophobicity so that the gel will not leak out into the medium channels during gel filling. After 24 h, the gel is similarly mixed as a liquid phase and kept over ice in an eppendorf tube. 10 µl of hydrogel solution is pipetted into the device through the gel filling port. To improve the uniformity of the gel structure upon polymerization, half of the gel chamber should be filled through one gel filling port. Then, the pipette should be removed, and the remainder of the gel chamber should be filled through the opposite gel filling port. For a detailed protocol of the gel filling process, and rationale for the design and dimensions, see Farahat et. al., 2012.[16]

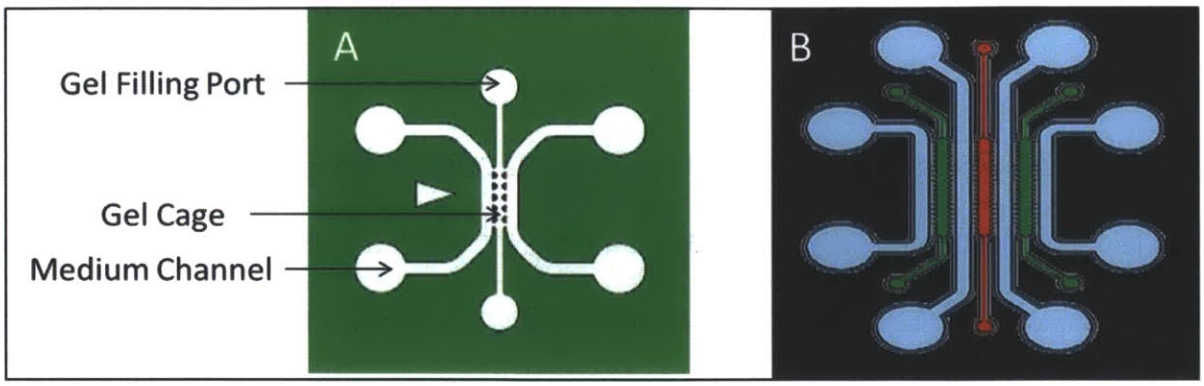

Figure 1. Two designs implementing the gel filling port system. (A) Single gel cage design. (B) Triple gel cage design. Gel is filled using standard pipette tips through the gel filling port. Posts on either side of the gel cage prevent the gel from leaking into the medium channels. Medium is added to the side channels after gel polymerization to provide nutrients and maintain hydration of the system. Cells can be cultured in the gel or in the channels and induced to migrate into and through the gel.

Comparison

The major advantage of using the micro-injection system is the ability to maintain uniform gel structure during the filling and polymerization process. When filling through gel filling ports, the flow properties can impact the gel structure causing the protein filaments to align in the direction of flow. Additionally, the flow properties through the center of the gel channel can differ from the side regions in between the posts leading to further non uniform properties. These can be alleviated through filling the device slowly and using the two-step approach of filling each half of the gel chamber separately from its corresponding gel port as described above. An additional advantage of the micro-injection technique is realized when incorporating large objects into the gel as described in Chapter 3 in which alginate beads on the order of 100 μm were mixed into the gel. Attempting to squeeze these objects through a gel filling port could lead to a non-uniform suspension or could potentially damage the beads. However, the micro-injection system is subject to greater variability. There is little room for error in filling

exactly the right volume of gel into the gel chamber. Too little, and air will get trapped when the device is sealed with a coverslip; too much, and the gel will spill out into the medium channel. Finally, in contrast to the micro-injection system, the gel filling port system does not require any additional equipment. For these reasons we adopted the gel filling port system for the vast majority of applications.

Chapter 3: Vascularization Strategies

We successfully utilized two fundamental strategies for vascularization using our microfluidic platform: **(1)** angiogenesis and **(2)** vasculogenesis. Angiogenesis is the process whereby new blood vessels sprout from a pre-existing vasculature. This process occurs during the normal healthy functioning of an organism as well as during pathological conditions such as the vascularization of cancerous tumors. Vasculogenesis takes place mainly in the embryo during development. In this process, a mono-dispersed collection of endothelial or endothelial precursor cells spontaneously forms a nascent interconnected network of endothelialized tubes which differentiate and mature and ultimately form the basis for future vasculature that develops through angiogenesis.

Angiogenesis

Based on extensive work from our lab studying the initial formation of angiogenic sprouts from a confluent monolayer,[11–13] we hypothesized that we could use angiogenic growth factors to induce these sprouts to form hollow lumen structures which extended across the entire gel region. Experiments were performed by first filling the gel chamber with a collagen or fibrin hydrogel. Since the formation of a polymerized hydrogel is a dynamic process taking several hours to reach its final chemical and mechanical structure, we allowed 24 h for the gel to fully polymerize before seeding endothelial cells in the medium channel.

Seeding

After 24 h we introduced 20 µl of a cell suspension of endothelial cells in medium at a seeding density of 1-3 million cells/ml into one of the medium channels. To ensure that the endothelial cells (ECs) coated the vertical interface between the gel and the medium channel we employed one of two methods: **(1)** tilting or **(2)** interstitial pressure. For the tilting method, the seeded devices were tilted at 45 degrees for 30 min in the incubator to allow the cells to settle on the vertical gel surface before returning the devices to their horizontal position and filling the channels with fresh medium. Alternatively, we set up an interstitial pressure across the gel by filling an extra 20 µl of medium in the EC channel. This pressure forced ECs up against the vertical interface effectively enough to coat the surface and ensure a uniform monolayer. Non-uniform seeding proved to be the greatest drawback of the angiogenesis model. A bubble trapped in the medium channel frequently blocked the uniform flow of the cell suspension leading to patches of non-coated surface. The effectiveness of sprouting was highly correlated to the uniformity and extent of initial EC seeding. We found that the interstitial method was more consistent in general than the tilting method in our experiments. For a detailed protocol of the seeding procedure, see Vickerman et. al., 2008.[15]

Angiogenesis Device

Based on our findings that the integrity of the gel/medium interface is crucial to achieving effective and uniform sprouting, we opted to use a gel filling port design for sprouting experiments. The initial design for the gel filling port device called for a 1.3 mm wide gel cage.

We found that vascular sprouts in our system grew at a rate of roughly 100 μm per day. Since the ultimate goal of our system was to generate perfusable microvascular networks spanning the entire width of our device, we sought to decrease the width of the gel cage in order to decrease the time for complete vascularization. To contain the gel within the gel chamber using the gel filling port design, a balance must be maintained between fluid pressure pushing the gel out into the channels during filling and surface tension keeping it in between the posts. The former effect can be controlled by the length and width of the gel chamber while the latter can be controlled through adjusting the inter-post spacing. As the width of the gel region is reduced, it becomes difficult and ultimately impossible to keep the gel contained using surface tension alone. Through modeling and some trial and error, we altered the overall length and the inter-post spacing to allow for a reduction of the overall width to 500 μm. This decreased the time to full vascularization by over 50%. An alternative approach to decreasing the time to full vascularization was to seed both channels with ECs and simultaneously induce sprouting from both sides. This would presumably reduce the vascularization time by half as the opposing sprouts would meet and anastomose in the middle. After experimentation, however, we found that sprouts from neither side reached the middle of the gel chamber. Initial sprouts did form, but they quickly stalled and failed to progress. This was likely due to the fact that angiogenic sprouts respond to gradients in growth factor concentrations. When seeding only one channel with ECs, a higher concentration of vascular endothelial growth factor (VEGF) and other growth factors can be maintained in the opposing channel, inducing sprouts to form toward the empty channel. Even if no chemokine gradient is continuously maintained, it is likely that a natural gradient arises in the system. This is due to the fact that ECs in one channel

consume the growth factors there, leaving a higher concentration in the other channel. However, when both sides are seeded, the symmetry of the system does not allow for these gradients to form, and no spatial guidance cues exist to direct the sprouts.

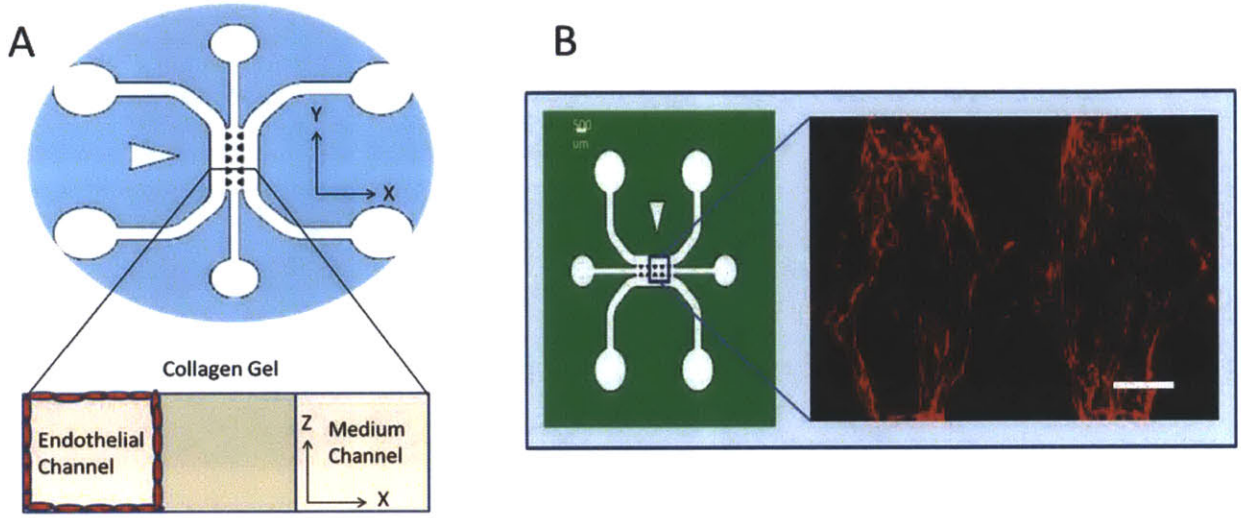

Figure 2. (A) Diagram of the angiogenesis gel-filling port device. Endothelial cells are seeded in one channel to form a confluent monolayer and induced to sprout through the gel by means of chemokine gradients. (B) Representative results using the device. Scale = 100 µm.

Results

Figure 3 demonstrates typical results using the angiogenesis method for vascularization. Typical time for vascularization in this device is 3-5 d. As demonstrated using confocal imaging, patent lumen structures extended throughout the entire 500 µm gel region. They were also distributed throughout the vertical z dimension, showing preference, however, for the surface closest to the glass coverslip. To further prove the perfusability of the networks, 10 µm microspheres were perfused through the system and their flow path was contained within the endothelialized lumen structures.

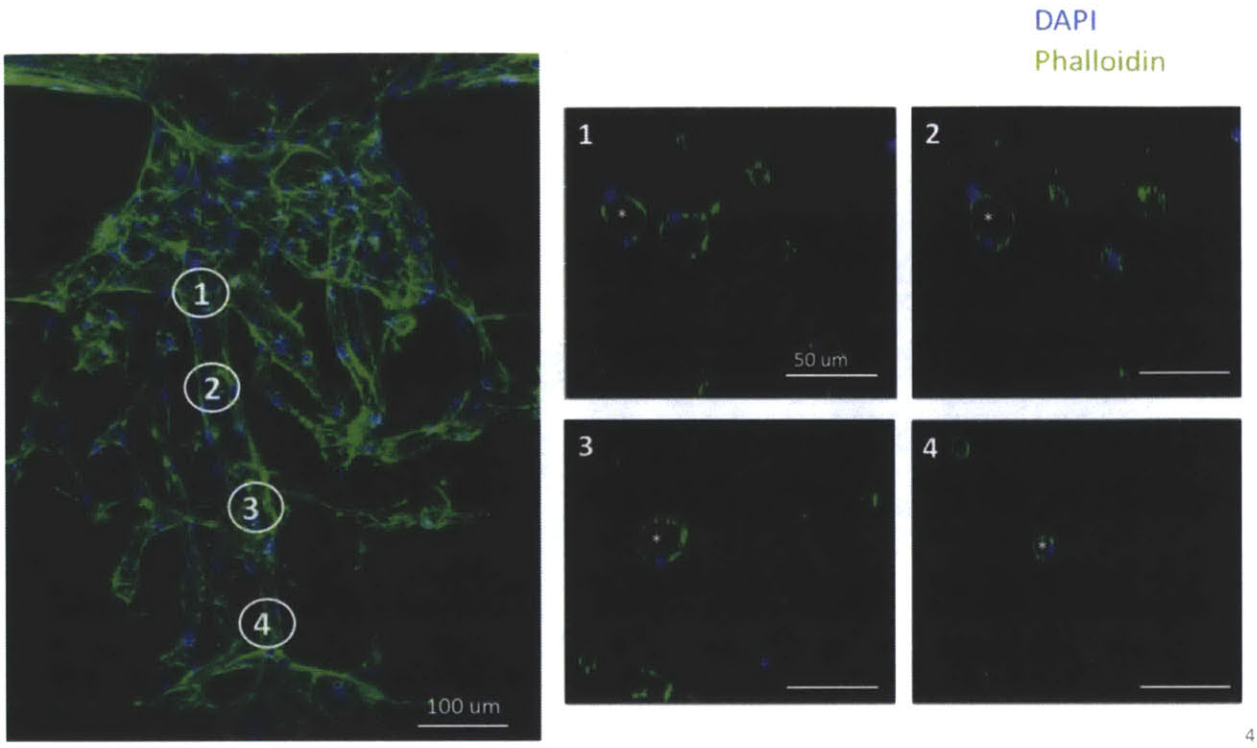

Figure 3. Confocal images of perfusable microvascular network formed using angiogenic sprouting method. Devices are fixed and stained for actin (green) and nuclei (blue).

Typical diameters of the vessels ranged from 10-30 μm which is on the high end of the range for capillaries but on the low end for other in-vitro engineered blood vessels.[17–19]

Alginate Beads

Based on our finding that vessels preferentially formed in the gel region closer to the glass coverslip, we attempted to further increase the uniformity of the z-distribution of vessels by incorporating stiff particles into the gel to act as a scaffold for the invading vessels. We chose to use alginate beads because they are bio-compatible and porous to chemokine diffusion, and their stiffness can be easily controlled by the concentration of alginate used. See Chan et. al.,[20] 2011 for a detailed study of these mechanical properties. Additionally, alginate has been used

to encapsulate cells for cell therapy applications, and the viability of the cells has been verified.[21] This enables us to incorporate a second cell type into the system in addition to ECs while still maintaining a spatial segregation between the cell types.

Bead Forming Methods

We employed two different methods for producing alginate beads: **(1)** air-cutting and **(2)** two phase microfluidic device. Air-cutting is simple and enables large quantities of beads to be formed in a short amount of time. However, it is difficult to control the size distribution of beads with precision. The two phase microfluidic device enables precise control of the bead size based on the flow rates of the syringe pumps. However, three syringe pumps must be used and the production rate is much slower.

Air-Cutting

The air-cutting technique utilizes a syringe pump to extrude the alginate solution while a filtered air stream from above cuts the solution, sending alginate droplets into a calcium bath positioned below the stream. The calcium instantaneously crosslinks the alginate producing stiff, spherical, alginate beads. The beads are then rinsed of excess calcium and can be filtered to collect only beads within a desired size range. For a detailed protocol, see Chan et. al., 2012.[22]

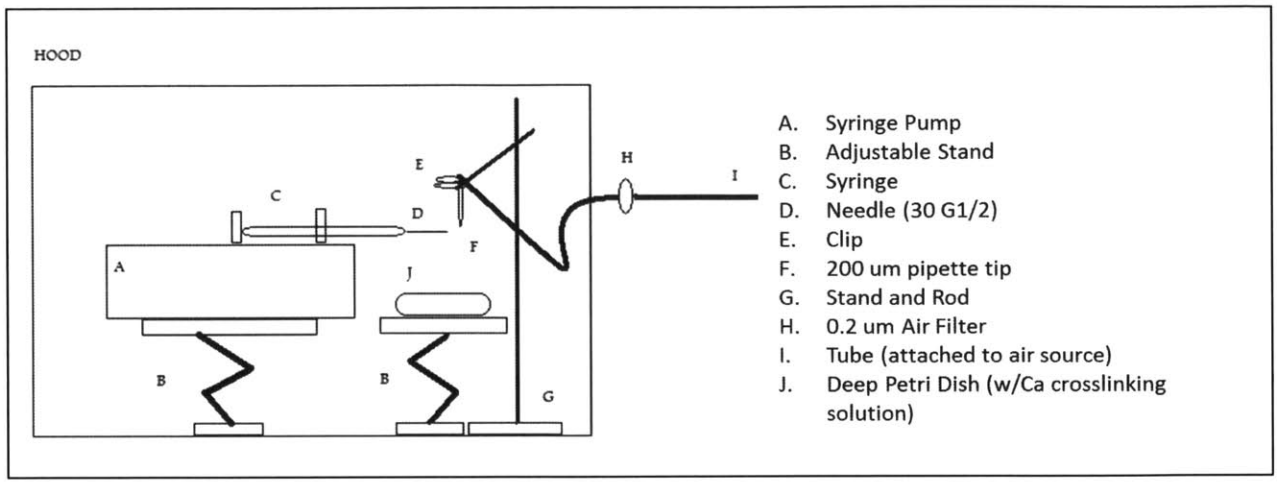

Figure 4. Schematic diagram of the air-cutting method for producing alginate beads. A syringe pump extrudes alginate solution while an overhead air stream cuts the alginate stream into spherical particles which drop into a calcium cross-linking solution.

Microfluidic Two-Phase Device

Alternatively, we modified a previously published two-phase microfluidic device to produce a highly uniform collection of mono-dispersed alginate beads by flowing a 1% alginate solution down the central channel and cutting that flow into spheres using a solution of calcium and oleic acid. See Kim et. al., 2009 for a detailed protocol.[23] The size of the beads can be controlled by adjusting the flow rate of these two streams and can be calibrated with high precision. For experiments in which we encapsulated tumor or stromal cells within the alginate beads, these cells were suspended in the alginate solution. Because the oleic acid is harmful to cells, a third stream with mineral oil was introduced after the beads were formed and cross-linked in order to rinse off the acid. This step avoids the possibility of immediately detrimental effects to the encapsulated cells, but further rinsing is required after the cells are collected.

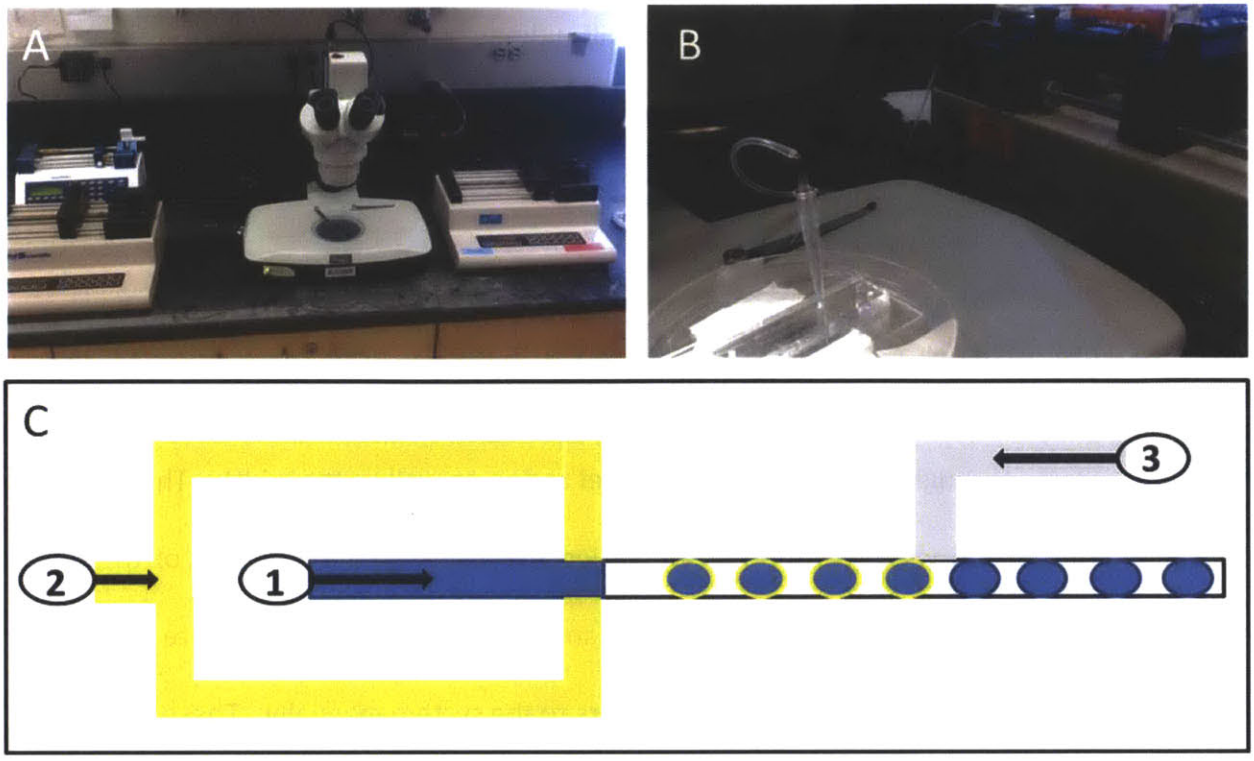

Figure 5. Setup of the two-phase microfluidic alginate bead making system. (A) three syringe pumps and a microscope are required. (C) Diagram of the two phase microfluidic device: (1) alginate solution (2) Calcium/Oleic acid crosslinking solution (3) mineral oil.

Comparison

As discussed above, the benefit of using the air-cutting method is speed and the need for only one syringe pump. However, it is more difficult to achieve a uniform size distribution of beads. The two-phase microfluidic device allows for precise control over the bead diameter, but it requires three syringe pumps which increases the cost and the preparation time. Additional drawbacks of the two-phase microfluidic system include the inability to increase the alginate concentration above 1% without clogging the system. Also, when including cells in the alginate solution for encapsulation, the cells tend to aggregate near the inlet after a short period of time. If the cells are not broken up by manually agitating the device, this will lead to a non-

uniform distribution of encapsulated cells and will ultimately clog the device. Based on the above considerations, the appropriate method should be utilized depending on the specific requirements of the application.

Results and Discussion

We found that the alginate beads did indeed act as a scaffold to induce a uniform distribution of vascular sprouts throughout the height of the gel region as well as the width. There was no noticeable difference in vascularization as we varied the alginate concentration of the beads between 1-4%. We also encapsulated fibroblasts in the alginate beads to secrete angiogenic factors rather than adding exogenous growth factors to the system manually. These results and methods are further elaborated in Chan et. al., 2012.[22]

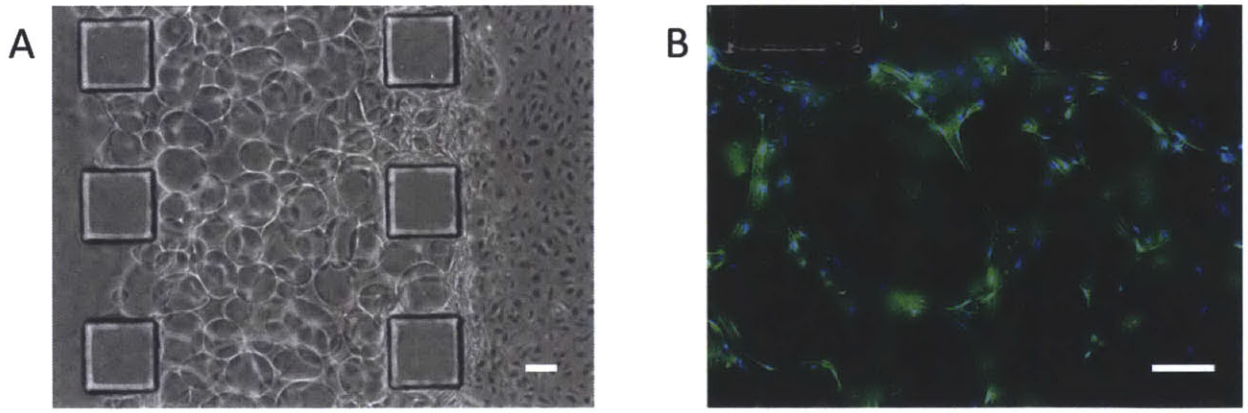

Figure 6. (A) Alginate beads mixed with collagen gel in the gel chamber. ECs are seeded as a monolayer in the right channel. Scale = 100 μm. (B) ECs invade the collagen gel following the path between alginate beads and forming perfusable networks. Scale = 100 μm. Green: phalloid; Blue: DAPI.

The mechanism by which the alginate beads induced this uniform z-distribution of vessels is still unclear. It is possible that the tip-cells were spatially confined to the collagen gel between the beads which were too stiff to penetrate. This spatial seclusion may have acted to guide the tip

cells through the collagen filled voids in a path that was randomly oriented in all three dimensions. Alternatively, the mechanism of durotaxis may have dominated by inducing the ECs to migrate preferentially towards and along the stiff surfaces of the alginate beads. These EC coated surfaces may have then formed the endothelial monolayer enclosing the observed patent and perfusable lumens. We again perfused the networks with <10 μm microspheres to demonstrate perfusability. To further demonstrate the functionality of these microvascular networks, we perfused the system with 150 kDa Dextran and observed it to remain within the endothelialized lumen structures. The semi-permeable barrier effect of the endothelial monolayer was confirmed by tracking the Dextran diffusion into the interstitial area over a 30 min period.

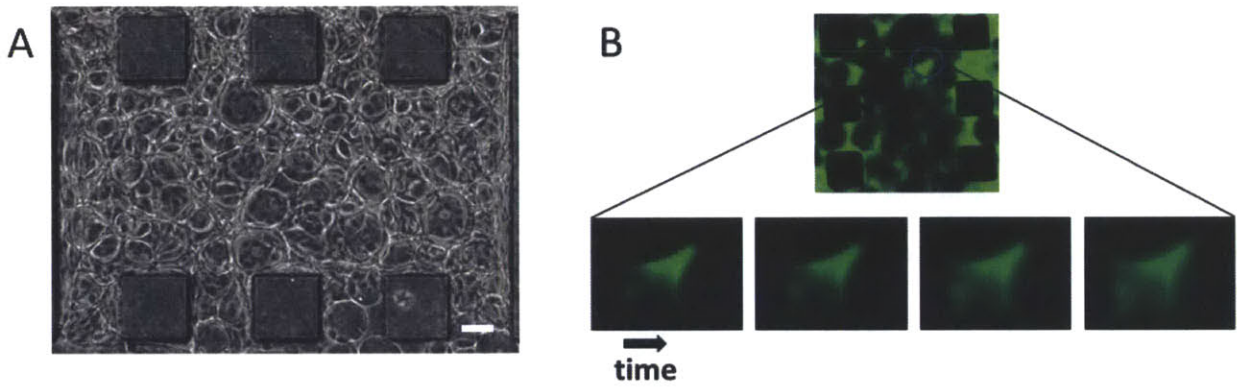

Figure 7. (A) 100-200 μm diameter alginate beads in a collagen gel filled into the gel chamber of a micro-injection device. Scale = 100 μm. (B) 150 kDa Dextran was flowed through the perfusable microvascular networks to test the barrier function of the endothelial monolayer. The dextran was initially contained within the endotheliazid structures and slowly diffused into the interstitial space.

Intermediate Post Device

In initial sprouting experiments using a device with a 1.3 mm wide gal chamber, we found that sprouts would form robustly, containing hollow lumens, for distances up to 500 μm. At that

point, the tip cell would repeatedly break off from the stalk, and the stalk cells would subsequently disassemble from their structure leaving nothing but individual, disconnected ECs. Based on our findings from the alginate bead experiments, we hypothesized that intermediate stiff structures throughout the gel region may help to guide the sprouts and provide anchor points for the vessels to maintain their structure while traversing the entire width of the gel.

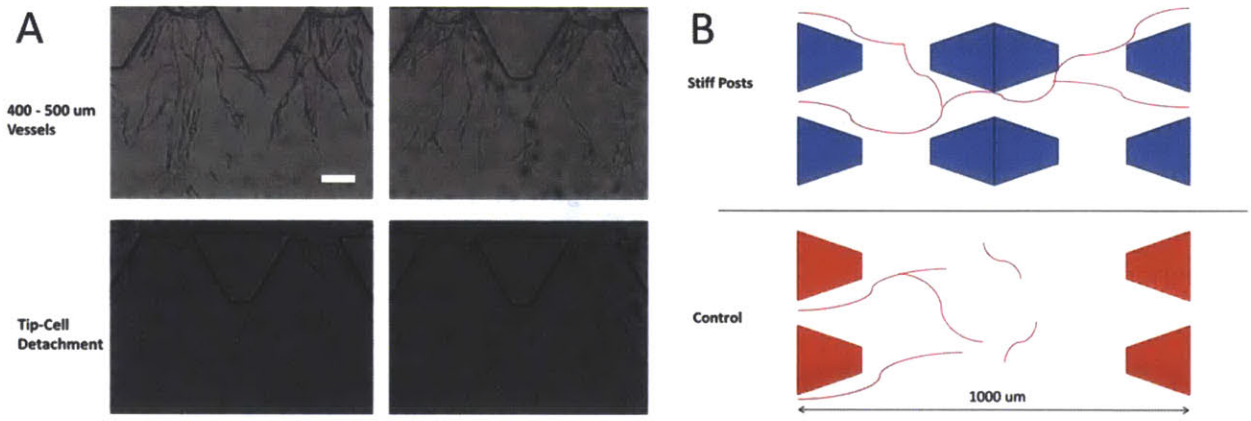

Figure 8. (A) Experiments using a 1.3 mm wide gel region showed that tip cells would detach after 500 um of sprout formation leading to disruption and regression of the sprout. (B) Intermediate rows of posts were introduced to provide guidance and anchorage for invading sprouts to traverse the entire gel region.

To test this hypothesis, we used a device containing several rows of staggered posts within the gel chamber. These PDMS posts provided guidance and direction to the invading sprouts. We found that the posts did indeed facilitate full length sprouting across wide regions of collagen gel. We used devices with 3 and 5 rows of posts and found that the morphology of the networks was dependent on the layout of the posts.

Figure 9. (A) Phase image of the 5-row intermediate post device. Scale = 1 mm. (B) Stained image of microvascular networks traversing the entire width of the 3-row intermediate post device. Scale = 0.1 mm. Red: phalloidin Blue: DAPI (C) 20X image of a vessel using the posts as anchorage. Scale = 0.1 mm.

By designing the post layout, which indirectly determines the design of the inter-post gel geometry, the diameter and morphology of the networks can be controlled. It is also possible to effectively control the network morphology by varying the diameter of alginate beads in the above method which, again, determines the inter-bead gel geometry. The intermediate post method provides more accurate control. However, each design requires its own silicon mold; making it costly and time consuming to implement this method robustly. A drawback of this method is that the collagen gel often becomes separated from the posts as invading ECs probe and contract the gel. This can lead to highly inconsistent gel properties throughout the device and produce large gaps in the gel making it difficult to apply flow once the networks have formed.

Vasculogenesis

Vascular networks can also form through the process of vasculogenesis. This is typical during the initial development stages of an organism when individual ECs or Endothelial pre-cursor cells extend protrusions to connect to neighboring cells. They form a highly interconnected

network, eventually maturing into multicellular tubular structures with patent lumens. This initial network is further pruned during maturation and the initiation of shear flow.

To mimic the process of vascularization in our microfluidic device, we mixed ECs as a single cell suspension within a collagen or fibrin hydrogel during the gel filling process. We found that ECs spontaneously formed interconnected networks within the first 24 h. Between 2-3 d, the EC tubes progressed into hollow structures with patent lumens. By day 4, we were able to perfuse the system. For a detailed protocol and reagents list, see Appendix I.

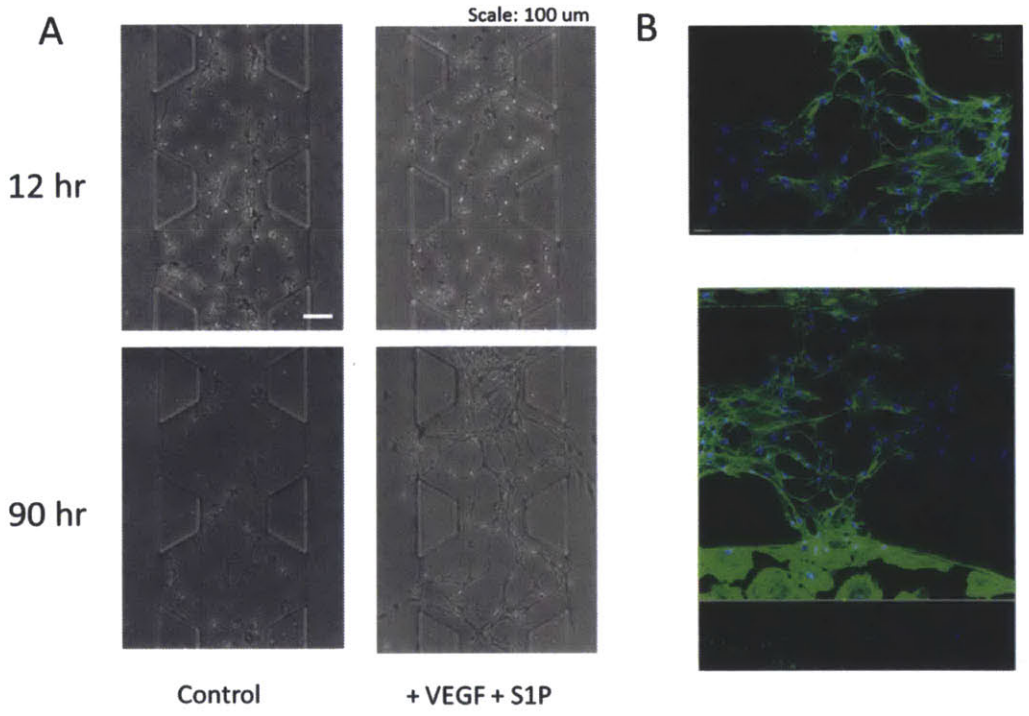

Figure 10. (A) Vasculogenesis experiments: seeding HMVECs in a collagen gel. Additional growth factors were required to produce and sustain interconnected networks. Scale = 100 μm. (B) Images of vascular networks formed using the vasculogenesis technique. Green: phalloidin; Blue: DAPI.

Interestingly, we observed a difference in behavior between human umbilical vein endothelial cells (HUVECs) and human microvascular endothelial cells (HMVECs) in their ability to form vascular networks through the process of vasculogenesis. Whereas HUVECs robustly formed

vascular networks within the first 24 h and almost all the cells survived the gel polymerization process, HMVECs often only formed networks after 24 h and many dead cells were observed in the gel. By adding VEGF and sphingosine-1-phosphate (S1P) to the medium we were able to produce more robust network formation that lasted through day 4. With HUVECS, no additional growth factors were required to maintain the networks through day 4. However, using both cell types, we found that the networks regressed after 4 d even with the addition of exogenous growth factors. This issue was addressed and successfully solved by the additional co-culture of fibroblasts as described in Chapter 4.

Comparison

We successfully employed three different strategies for vascularization using our microfluidic platform. Each system provides its own advantages and is best suited for specific applications.

Table 1. Comparison of the three vascularization techniques demonstrated using our microfluidic platform.

Method	Advantages	Disadvantages	Application
Alginate Bead Scaffold	• 3D vascularization • Encapsulation of secondary cell type	• Limited interstitial volume • EC coated surfaces vs. physiological lumens	• Tissue engineering • Biological machines
Vasculogenic Network Formation	• Closed network • Fast network formation • Reproducibility	• 2D networks	• Extravisation • Tissue engineering • Biological machines • Emergent behavior modeling
Angiogenic Sprouting	• 3D Vessels • Perfusable	• Flow not contained to vessels • High variation	• Angiogenesis • Biological Machines

A major advantage of the vasculogenesis method is the speed at which vascular networks form. Perfusable networks can be obtained after 3-4 d, but they are mostly contained to a single plane. Also, the networks are highly interconnected, and do not contain many dead-end channels as is typical of the networks formed by angiogenesis due to the detachment of tip cells. The high degree of interconnectivity ensures that objects perfused through the networks will remain contained within the networks. For this reason, the vasculogenesis method was used to create networks for extravasation studies in which cancer cells were perfused through the network and observed as they transmigrated through the endothelium into the interstitial tissue area.[24] The alginate bead method is ideal for tissue engineering applications in which the major cell type of a specific tissue can be encapsulated while the vascular network delivers oxygen and other nutrients. In cases where accessibility to the region in need of vascularization is limited, the angiogenesis method must be employed and the invading sprouts should be directed toward the undernourished tissue.

Chapter 4: Control of Microvascular Network Morphology

Engineered biological tissue for implantation and regenerative therapies requires a functional microvasculature to ensure proper function and survival in its intended working environment. It is likely that the desired microvascular network (MVN) morphology of an engineered tissue will vary depending on its ultimate function in the body. This can be inferred from the significant differences found in the microvasculature of various organs in-vivo and across species.[25] With this in mind, Hoganson et al.[26] applied a biomimetic design approach to the tissue specific microvascular requirements of the liver. Additionally, many mathematical models – originating with the theory set forth by Murray[27], based on the principle of minimum work - have been developed to determine the optimal design of a microvascular network[25,28–30]. However, these designs have generally been implemented in the form of preformed vascular molds which are subsequently seeded with endothelial cells[31] and thus do not mimic the complex process of vascular network formation in-vivo. There has been remarkable progress recently in forming perfusable microvascular networks in three-dimensional hydrogels without the need for artificial architecture to support the vascular structures[19,32,33]. Still lacking, however, is a systematic study of the factors controlling network morphology and the effects of signaling between different cell types.

Moreover, the dominating influence determining network morphology is generally assumed to consist of fluid flow dynamics and related shear forces acting on the endothelium. However, it has long been recognized that mechanical and biochemical properties of the microenvironment can also play important roles in determining MVN morphology. The goal of our research was,

therefore, to probe the biochemical and mechanical environment of endothelial cells undergoing the processes of angiogenesis and vasculogenesis in a three-dimensional hydrogel to determine the influence of these factors on the morphological characteristics of the resulting engineered MVNs. By uncovering these design principles, we are able to take advantage of the natural control mechanisms employed in-vivo to guide MVN formation towards a desired morphology.

Angiogenesis

Effects of Extracellular Matrix

In addition to the importance of cell-cell interactions to the normal and pathological functioning of tissues, it is also known that the cell-ECM interactions can heavily impact cellular function. Our microfluidic device lends itself to studying these cell-ECM interactions in a precisely controlled and quantitatively observable manner.

ECM Composition

We have successfully used fibrin, collagen, and PEG gels for cell encapsulation in our microfluidic device. We found that sprouting angiogenesis is similarly robust in both fibrin and collagen gels at equivalent protein concentrations (2.5 mg/ml). For vasculogenic network formation, we found fibrin gels to be most suitable. When seeded in collagen gels, HUVECs quickly contracted the gel, pulling it away from the retaining posts and causing the system to collapse in on itself. The properties of fibrin gel are such that the fibers are highly extensible up to considerable strains.[34] This allows the network forming ECs to pull and contract the gel without disrupting its overall structure.

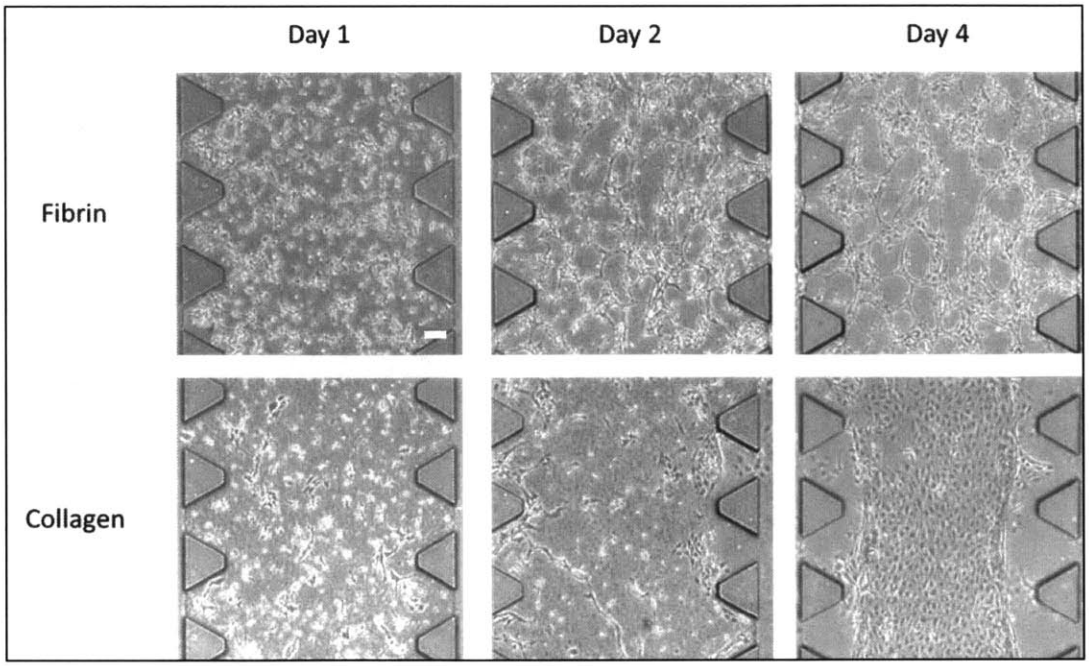

Figure 11. Vasculogenesis experiments with HUVECs seeded in either fibrin or collagen gel. ECs in collagen contracted the gel and were unable to form organized networks. Scale = 100 μm.

PEG gels were used due to their high stiffness potential and the ability to functionalize the fibers with highly specific peptides. Stiff PEG gels provide an alternative to the alginate bead strategy discussed in Chapter 3 for encapsulating secondary cell types while restricting their migration capabilities. We also accomplished this by designing PEG gels with variable degrees of degradable cross-linkers. We used this strategy to control the rate at which encapsulated fibroblast cells could migrate away from their cell-specific sequestered gel region and into the EC inhabited gel region. This enabled us to include contact and non-contact co-culture conditions within the same device, which is typical of vascular network formation in-vivo in which stromal cells first communicate with ECs by secreting diffusible factors and are later

recruited to form stabilizing cell-cell contact interactions.[35] For a detailed protocol for PEG gel preparation, see Raeber et. al., 2005.[36]

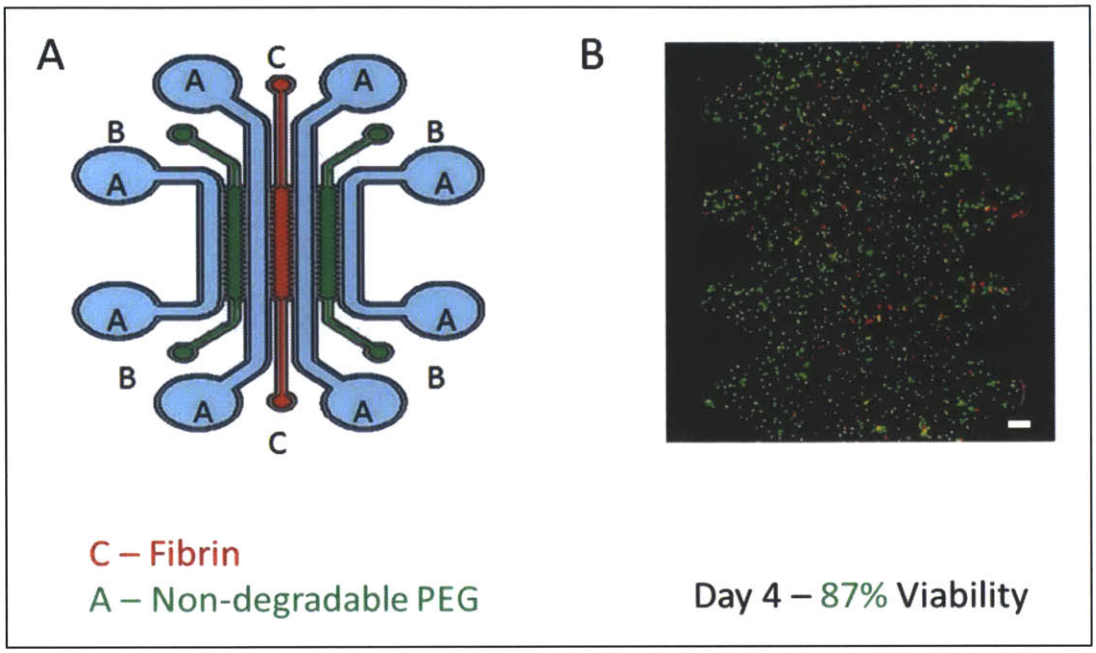

Figure 12. (A) Diagram of three gel-region device. Secondary cells are immobilized in stiff, non-degradable PEG gels from which they secrete factors needed by ECs to form vascular networks. (B) Live (green) and dead (red) staining of fibroblasts encapsulated in PEG gel confirms their viability. Scale = 100 μm.

Collagen Gel Stiffness

It is possible to control the stiffness of collagen gel by altering the concentration of collagen present and the pH of the solution during polymerization (for a detailed protocol, see Yamamura et. al., 2007)[37] – among other methods[38]. We chose to increase the stiffness in our system by increasing the pH as opposed to increasing the collagen concentration in order to isolate the mechanical effects as much as possible. By adding more collagen, the amount of cell adhesion ligands also increases and this could introduce compounding biochemical signaling effects to the experiment.

It should also be noted that increasing the pH of the solution during polymerization also decreases the pore size of the fibrous network structure. Therefore, it could be a combination of stiffness and pore size effects giving rise to altered vascularization dynamics in our system.

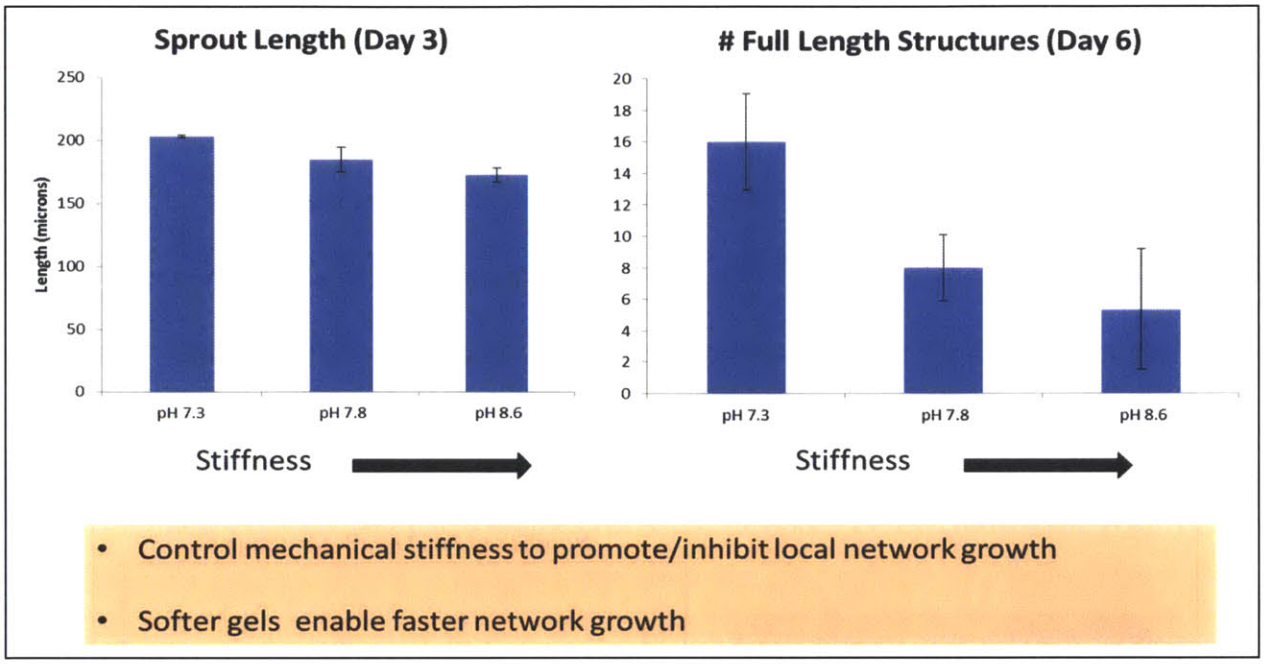

Figure 13. The speed of vessel growth as measured by the rate of advancement of the tip cell as well as the final number of perfusable vessels was inversely related to increasing collagen gel stiffness.

We found that stiffer gels inhibited vascularization during angiogenic sprouting in our system. The rate of sprout growth as well as total number of perfusable sprouts spanning the entire gel region was inversely related to the increasing stiffness of the gel. This stiffness dependence could be used as a control mechanism to induce or inhibit angiogenic sprouting, for instance, in order to supply blood flow to ischemic regions of the heart or the limbs of diabetic patients, or to prevent the vascularization of cancerous tumors.

Growth factors

We also studied the effects of soluble biochemical factors on the process of angiogenic network formation. To this end, we divided the process into two separate parts: 1) initial sprout formation and 2) long-term maintenance. This was due to our observations that even full length sprouts would regress after several days; eventually breaking apart into individual cells. Much research has been done to decipher the molecular and signaling mechanisms which guide the various stages of angiogenesis.[39] We chose the primary growth factors known to play a critical role in these two separate stages of angiogenesis in an attempt to re-create the entire process from initial sprouting to long term maintenance of quiescent vessels.

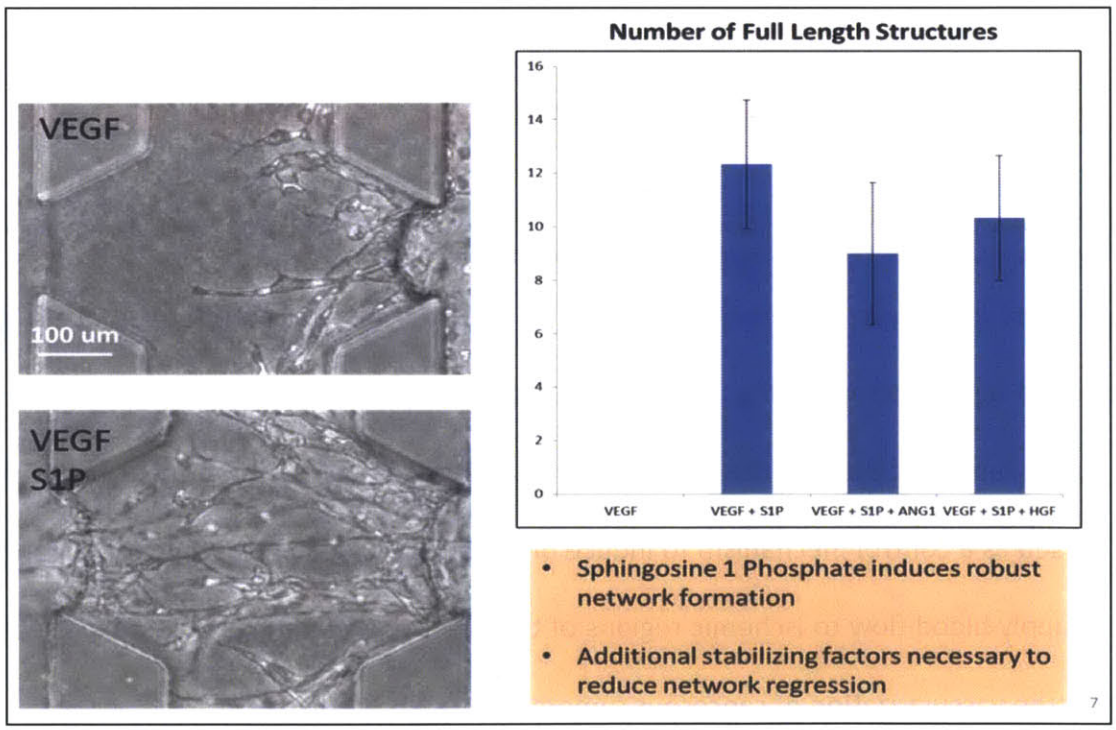

Figure 14. Supplementation of the growth medium with S1P was necessary to induce robust sprouting in our angiogenesis model. ANG1 and HGF, known stabilizing factors, did not increase stability of the vessels in our system as measured by the number of full length vessel structures to remain after 2 d of prolonged culture after vessel formation.

VEGF is the most well-known and studied angiogenic growth factor. Interestingly, we found that VEGF alone (50 ng/ml) was not sufficient to promote robust sprouting. In our system, sprouting critically depended on the presence of Sphingosine-1-Phosphate (S1P). S1P is an interesting angiogenic growth factor in that it acts as both a migratory cue to initiate sprouting at early stages and as a stabilizing factor to induce quiescence at later stages.[40] We found that S1P (250 nM) induced robust sprouting in a dose dependent manner.

To solve the problem of vessel regression, we applied the growth factors hepatocyte growth factor (HGF; 50 ng/ml) and angiopoietin-1 (ANG-1; 300 ng/ml) which are proven stabilizing factors during angiogenesis.[39,41] Stabilizing factors work in one of two ways: 1) directly promoting strong junctions between ECs or 2) recruiting stabilizing cells to cover the outer surface of the vessels. The chosen stabilizing factors function by the first method and should operate effectively in our system even though stabilizing cells are not present. We did not, however, observe any noticeable stabilizing effects of these growth factors. There was no increase in the number of full length structures as compared to the case where only angiogenic sprouting factors were applied; the vessels regressed at the same rate. Most likely, this persistent regression was due to the lack of secondary stabilizing cells in our system. It is also possible that the vessels regressed because they did not sense the stabilizing effects of shear flow which are present in physiological quiescent vessels.

Interstitial flow

A defining feature of our microfluidic platform, and one of its major advantages over standard petri-dish and well-plate cell culture experiments, is the ability to apply prescribed flow

conditions. We know that the forces experienced by cells due to interaction with flowing fluids can affect their internal biological processes; this phenomenon is known as mechanobiology.[42] Shear forces on the endothelium due to flow through capillaries has a stabilizing effect on them, and abnormal flow conditions can lead to pathological functioning as in the case of atherosclerosis.[43] In our lab, interstitial tissue flow has been shown to affect tumor cell migration and to act as an angiogenic switch during sprouting angiogenesis.[11,44] The effects of interstitial flow on vascular network formation have also been reported by Song and Munn, 2011[45] and by Moya et. al., 2013.[33] We sought to take advantage of this migration inducing effect in order to control the entire process of vessel formation in our device beyond the initial sprouting step. To accomplish this, we inserted reservoirs into the medium ports on both sides of the gel region and introduced a hydrostatic pressure drop across the gel by filling the ports to different heights. For a detailed protocol, see Polacheck et. al., 2011.[44]

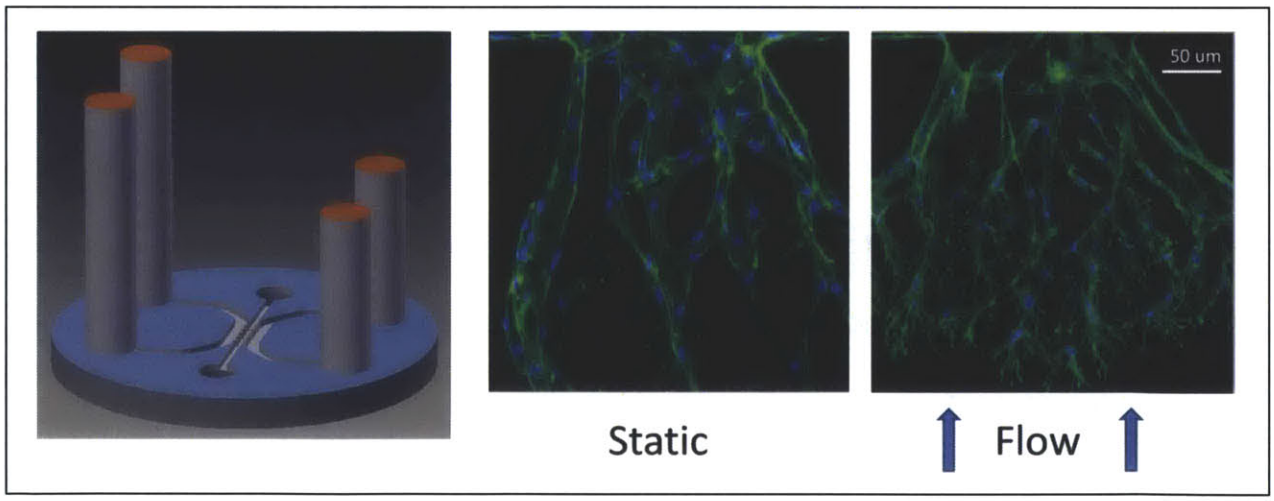

Figure 15. Reservoirs were inserted into the medium channel ports and filled to different heights to impose a hydrostatic pressure induced flow across the gel. Under flow conditions, sprouts were more branched and tip cells contained more filipodia.

By applying flows at speeds up to 100 μm per second, we were able to induce robust sprouting which was sustained by the growing vessels as they extended fully across the gel. The networks formed under interstitial flow conditions were more branched than the control case. They contained more tip cells, and those tip cells expressed more filipodia per cell. Thus, interstitial flow provides an additional mechanism that can be exploited to control the dynamics of engineered microvascular network formation and the morphology of those networks. Future studies should provide a detailed analysis of the mechanotransduction mechanisms at play and determine whether the flow effect is velocity dependent.

Vasculogenesis

To study the effects of the mechanical and biochemical microenvironment on the network morphology of vascular networks formed through the process of vasculogenesis, we used a multi-culture perfusable microfluidic platform enabling real-time observation and independent control over paracrine signaling, cell-seeding densities, and hydrogel mechanical properties (Figure 16 A-B). Human umbilical vein endothelial cells (HUVEC) were seeded in fibrin gels and cultured alongside – but not in contact with - human lung fibroblasts (HLF). HUVECs spontaneously formed networks within 24 hours and the engineered vessels contained patent, perfusable lumens as demonstrated by the passage of fluorescent microspheres after 4 d. Communication between the two cell types was necessary to avoid network regression and maintain stable morphology beyond 4 d. Fluorescent imaging and subsequent analysis was used to quantify the number of branches, average branch length, percent vascularized area, and average vessel diameter of the MVNs generated under various conditions. Finally, results were tabulated and the design parameter space was mapped out for the conditions studied.

This study provides quantitative results for direct use in the design of engineered microvascular networks. It also demonstrates the powerful capabilities of miniaturized, perfusable, three-dimensional engineered microvascular networks to study the influence of the multitude of environmental cues affecting network morphology in a high-throughput and readily observable manner. It more generally demonstrates the ability to approach microvascular tissue engineering as a design problem using systematic, quantitative analysis.

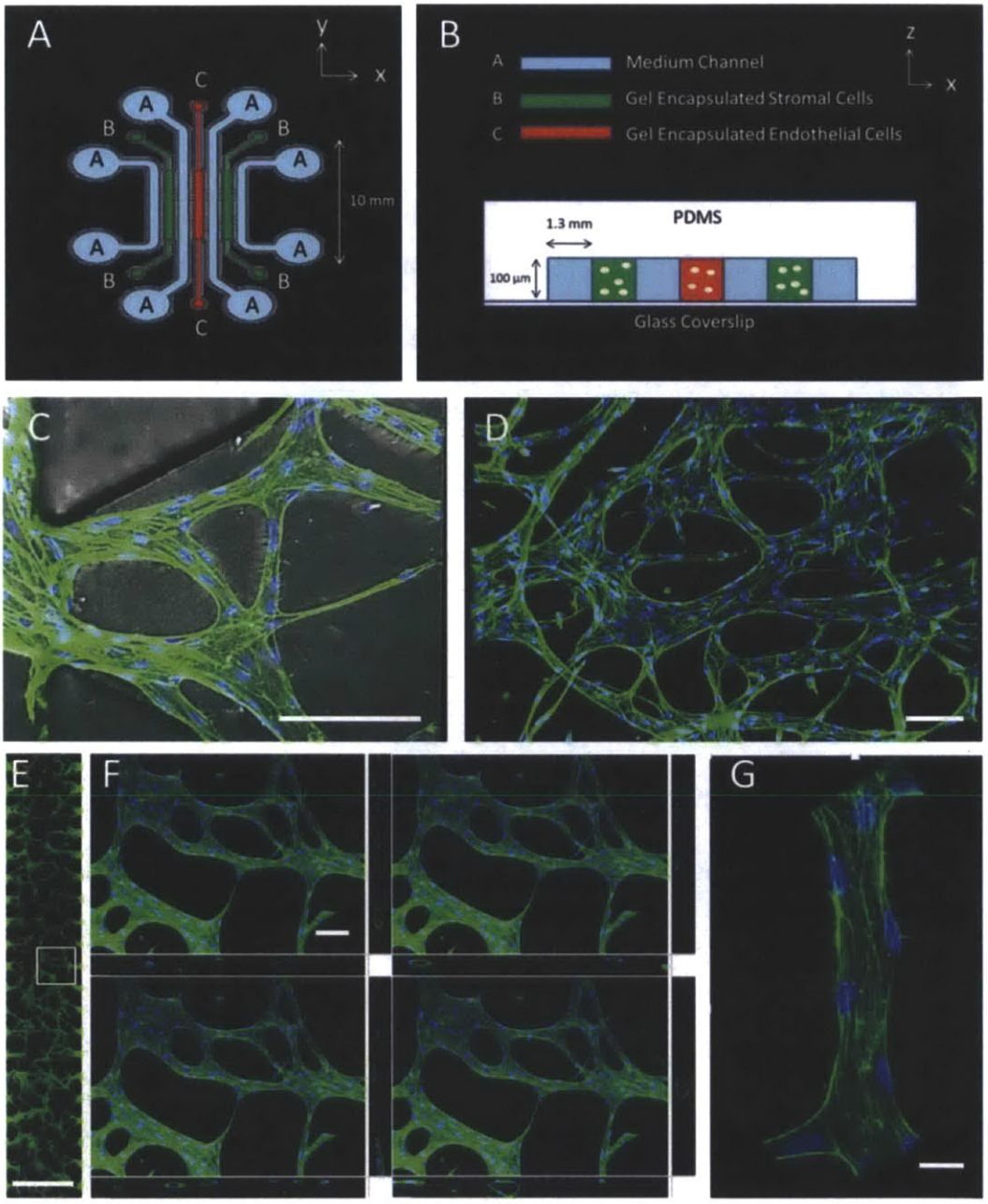

Figure 16. (A) Top view diagram of multi-culture microfluidic device containing three parallel gel regions for encapsulation of endothelial and stromal cells. Gel regions (B & C) are separated by medium channels (A) for gas exchange and delivery of nutrients. (B) Cross-sectional view diagram of multi-culture microfluidic device. Cell-culture region is surrounded by PDMS above and glass coverslip below (not to scale). (C) Top view of perfusable vessels opening to medium channel on left. Region shown is between two PDMS trapezoidal posts. 20 such regions exist in each microfluidic device. Staining: Green – phalloidin; Blue – DAPI (same for 1D-G). Scale bar = 100 µm. (D) 10X confocal image of perfusable microvascular network grown in multi-culture microfluidic device. Scale bar = 100 µm. (E) Full image of vascularized gel region. White box corresponds to enlarged image in 1F. Scale bar = 1 mm. (F) Sequence of four section views taken throughout 20X confocal stack. Vertical cross sections on bottom and right correspond to the location of the white crosshairs. These demonstrate the existence of patent lumens spanning the 100 micron height of the gel region. Scale bar = 100 µm. (G) 40X confocal image of segment of perfusable microvessel showing multiple cells. Scale bar = 10 µm.

Materials and Methods

Device Design

The design of this multi-culture vasculogenesis device was based on earlier designs from our lab[46] with some important adjustments: (1) a third parallel gel region was included so that stromal cells could be cultured on either side of the vascularized gel region (2) additional medium channels were included so that each gel region is flanked by two medium channels – one on each side – to provide adequate gas exchange and supply of nutrients and (3) the length of the device was increased from 2 mm to 8 mm to provide a larger region for vascularization.

To achieve optimal imaging conditions, we chose a height of 100 μm for the device and sealed it with a glass coverslip. This height enabled us to form generally planar perfusable networks, allowing us to capture the MVN morphological patterns from a single focal plane using epifluorescence. The height could be increased for clinical applications, in which it might be desirable to form vascularized tissue constructs containing several planes of vessels.

Cell Culture

Human umbilical vein endothelial cells (HUVEC; Lonza, NJ, USA) were cultured on collagen I coated flasks (50 μg/ml collagen solution in ascetic acid for 30 min; BD Biosciences, MA, USA) in EGM-2MV (Lonza, NJ, USA) growth medium and used in experiments between passages 6-8. Normal human lung fibroblasts (NHLF; Lonza, NJ, USA) were cultured in FBM-2 (Lonza, NJ, USA) growth medium and used in experiments between passages 6-10.

For exogenous growth factor experiments, EGM-2MV growth medium was supplemented with 50 ng/ml VEGF (Peprotech, NJ, USA) and 250 nM S1P (Sigma, MO, USA). Medium was replenished every two d.

Fibrin Gel Cell Encapsulation

Fibrinogen (Sigma, MO, USA) was dissolved in PBS (Lonza, NJ, USA) at twice the final concentration (2.5 – 20 mg/ml for fibrin concentration experiments). Thrombin (Sigma, MO, USA) was dissolved in PBS at 2 U/ml. These solutions were mixed, over ice, at a 1:1 ratio to produce a final fibrinogen solution with the desired concentration (1.25 – 10 mg/ml). The mixture was quickly pipetted into the device via the gel filling ports. The device was placed in a humidified enclosure and allowed to polymerize at room temperature for 10 min before fresh growth medium was introduced to the medium channels. Growth medium was replaced every two d.

For gels with encapsulated cells, a similar procedure was followed. Cells were spun down at 1200 rpm for 5 min and the cell pellet was re-suspended in EGM-2MV growth medium containing 2 U/ml thrombin and mixed with the fibrinogen solution at a 1:1 ratio. The device was placed in a humidified enclosure and allowed to polymerize at room temperature for 10 min before fresh growth medium was introduced to the medium channels.

Staining/Imaging

After 4 d, cells in devices were fixed with 4% paraformaldehyde (Electron Microscopy Sciences, PA, USA) for 15 min and rinsed 3X with PBS. 0.1% triton X (Sigma, MO, USA) was then introduced to permeabilize the cells and rinsed 3X with PBS after 15 min. The devices were then treated with DAPI and phalloidin (Life Technologies, NY, USA) for 2 h to stain the nuclei and actin respectively. Phalloidin staining was used to image vascular network morphology with an epifluorescent microscope (Nikon Eclipse Ti-S; Nikon Instruments Inc., NY, USA). Confocal images were taken with an Olympus IX81 microscope (Olympus America Inc., PA, USA).

Analysis/Quantification

The procedure used to process and analyze fluorescent images is described in detail elsewhere.[47] Briefly, raw images were prepared by enhancing contrast and removing noise. Automatic thresholding was used to binarize the images. Unconnected segments, which were not part of the perfusable networks, were automatically removed from the images. Finally, networks were skeletonized and analyzed[48] using image J software (http://rsbweb.nih.gov/ij/).

Effective diameter calculations were performed by dividing the thresholded vascularized area by the entire length of the skeletonized network.

For perfusability experiments with fibroblasts, the regions between PDMS posts containing vessels opening to the adjacent medium channels were counted and expressed as a percentage of the total number of regions.

Bead Flow Experiments

For bead flow experiments, vascular networks were fixed and stained as described above. Ten μm fluorescent microspheres (Life Technologies, NY, USA) were perfused through the networks by imposing a hydrostatic pressure drop across the endothelial cell gel region. Videos were recorded using NIS-Elements software (Nikon Instruments Inc., NY, USA) on a Nikon Eclipse Ti-S microscope (Nikon Instruments Inc., NY, USA) at a frame rate of 3.37 frames per second.

Statistical Analysis

All data shown represent experiments with at least n=3 individual microfluidic devices. Reported values correspond to averages over these devices for any given condition. Error bars were calculated using standard error. Significance was calculated using a two-tailed student-T test and p-values are supplied in Appendix II.

Results

Fibroblast Stabilization

In initial experiments, we used a microfluidic device with a single gel region seeded with ECs alone (see Chapter 3: Vasculogenesis). ECs alone did form vascular networks after two d of culture. However, these networks subsequently regressed with time. It has been shown that co-culture with fibroblasts enhances microvsascular network formation in sprouting angiogenesis[49,50], vasculogenesis[32] and in mixed co-culture experiments[33]. We suspected that fibroblasts in non-contact co-culture might also be important in stabilizing the nascent vascular networks before they regress. Using the revised multi-culture version of our microfluidic device

to encapsulate fibroblasts in the adjacent gel regions, we indeed found that the presence of fibroblasts effectively stabilized the microvascular networks as measured by total vascularized area and network perfusability (Figure 17). In the case of mono-culture, these properties gradually decreased after initial network formation, consistent with our preliminary experiments. However, under co-culture conditions, they reached a stable plateau after 4 d.

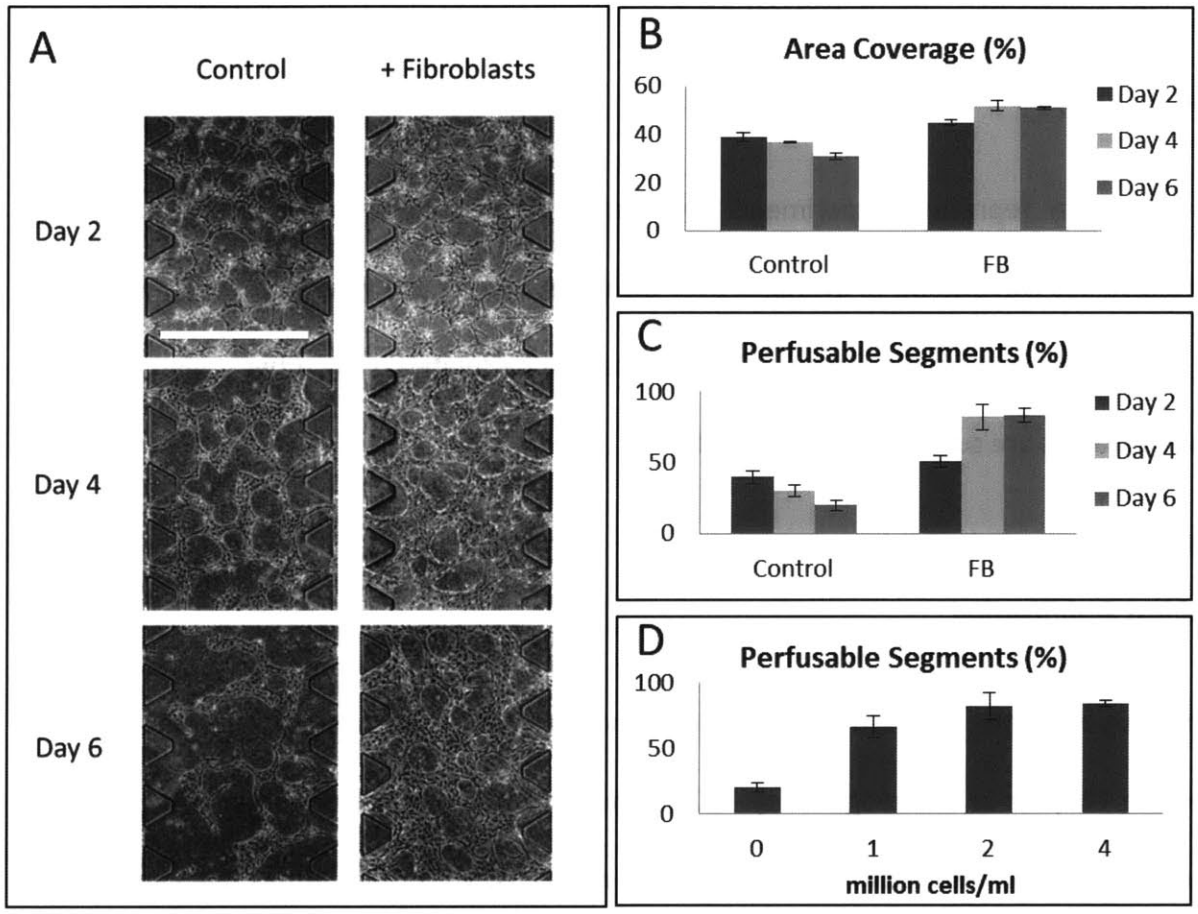

Figure 17. (A) 4X phase contrast images of microvascular networks formed by ECs in isolated mono-culture with complete medium (control) or in fibroblast co-culture with complete medium. After day 4, control networks regress while co-culture networks remain in-tact. Scale bar = 1 mm. (B) Area covered by microvascular networks under mono-culture and co-culture conditions over six day period. Values given are averages over at least 3 devices with error bars given as standard error (same for 2C-D). (C) Percentage of perfusable segments as defined by vascularized gel regions opening to medium channel containing at least one patent lumen. (D) Perfusable segments at day 6 as a function of fibroblast seeding density.

Paracrine signaling

In an attempt to recapitulate the stabilizing effects of the fibroblasts, pro-angiogenic growth factors – VEGF (50 ng/ml) and S1P (250 nM) – were added to the growth medium. We chose these growth factors and specific concentrations based on previous work in our lab in which they enhanced vessel sprouting and lumen formation in an angiogenesis model.[47] These growth factors did not significantly improve the long term stability of the networks. However, they did give rise to vascular networks with significantly different morphological characteristics.

The resulting networks contained more branches with shorter average length and smaller diameters than those cultured with fibroblasts or complete growth medium. The thinner structures in these networks covered less of the total area. Interestingly, by combining fibroblast co-culture with the supplemented growth factors, we were able to achieve the larger coverage area and network stability provided by fibroblast co-culture while maintaining the reduced diameters and average length induced by the angiogenic growth factors.

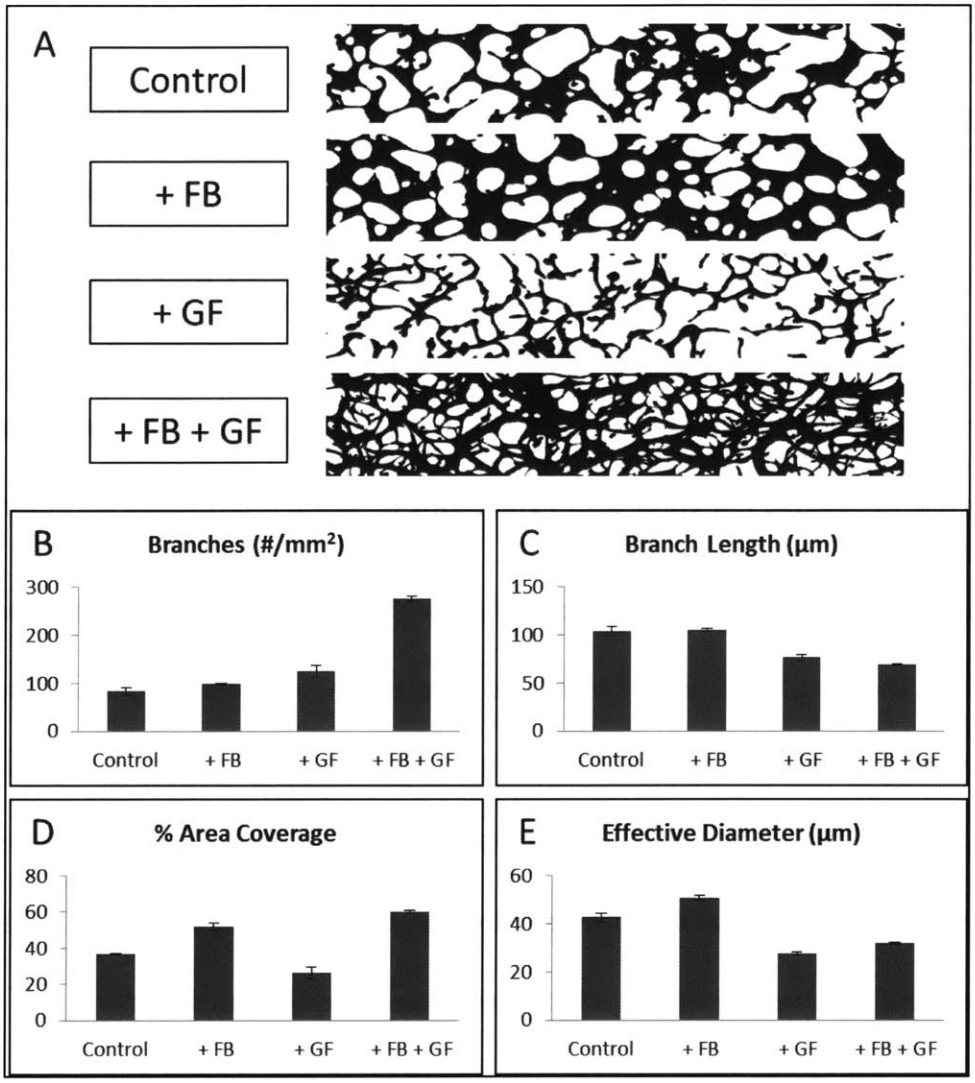

Figure 18. (A) Representative binary images of microvascular networks formed under conditions of: EC monoculture with complete medium; EC + Fibroblast non-contact co-culture with complete medium; EC monoculture with complete medium supplemented with VEGF (50 ng/ml) and S1P (250 nM); EC + FB non-contact co-culture with complete medium supplemented with VEGF and S1P. Fixed networks were stained with phalloidin and Imagej was used to process and binarize fluorescent images. (B) Number of branches per mm^2 of vascularized region. Values given are averages over at least 3 devices with error bars given as standard error (same for 3C-E). (C) Average branch length of microvascular network. (D) Percentage of area covered by perfusable microvascular network. (E) Effective diameter of vessels in engineered microvascular network, calculated as the ratio of vascularized area to total length of engineered microvascular network. P-values given in Appendix II.

Fibrin concentration

Fibrin gel was chosen for our experiments due to its biological relevance during tissue regrowth at wound healing sites and its unique mechanical properties. Specifically, fibrin gel

demonstrates strain-stiffening which allows it to be easily deformed by network forming ECs at small strains while maintaining its overall structural stability at the network level.[51] It is capable of undergoing large, recoverable deformations and can withstand considerably large strains before rupture.[34,52,53] We chose to alter the mechanical properties of our fibrin gel by varying the fibrinogen concentration from 1.5 to 10 mg/ml. Fibrinogen concentration is a key determining factor of the mechanical structure and strength of fibrin gels and has been shown to influence MVN formation.[54,55]

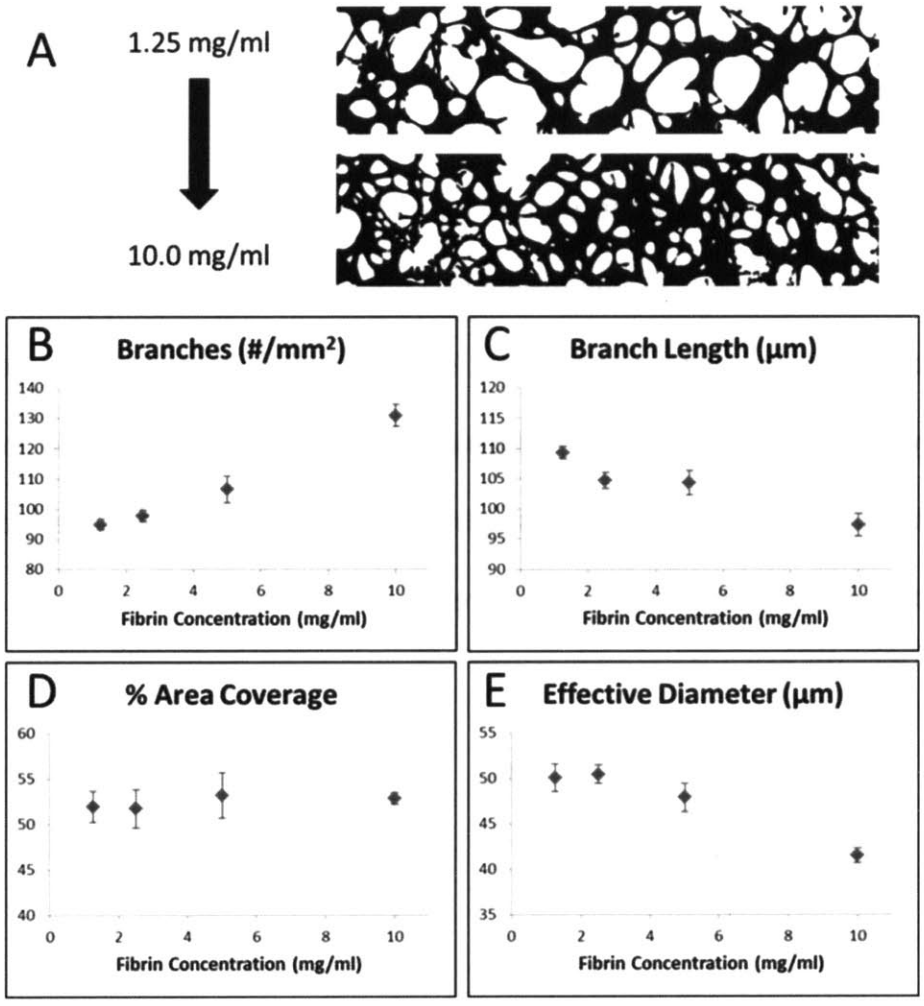

Figure 19. (A) Representative binary images of microvascular networks formed under conditions of increasing fibrinogen concentration for fibrin gel cell encapsulation experiments. Fixed networks were stained with phalloidin; Imagej was used to

process and binarize fluorescent images. (B) Number of branches per mm^2 of vascularized region. Values given are averages over at least 3 devices with error bars given as standard error (same for 4C-E). (C) Average branch length of microvascular network. (D) Percentage of area covered by perfusable microvascular network. (E) Effective diameter of vessels in engineered microvascular network, calculated as the ratio of vascularized area to total length of engineered microvascular network. P-Values given in Appendix II.

We found that the number of branches in a network was highly sensitive to fibrinogen concentration, while the coverage area remained little changed over the entire range of concentrations studied. Both the average branch length and effective diameter decreased with increasing fibrinogen concentration. The change in effective diameter between the two extreme conditions was 17.1 ± 4.6%.

HUVEC Seeding Density

We found that HUVEC seeding density plays an important role in MVN formation and the resulting network morphology. At one million cells/ml HUVEC seeding density, we found that sparse networks formed with comparatively short branches and small diameters. This represents the lowest seeding density achievable, beyond which perfusable microvascular networks will not form. With increasing seeding density, we found that the branch length, diameter, and area fraction of the vascularized region all increased.

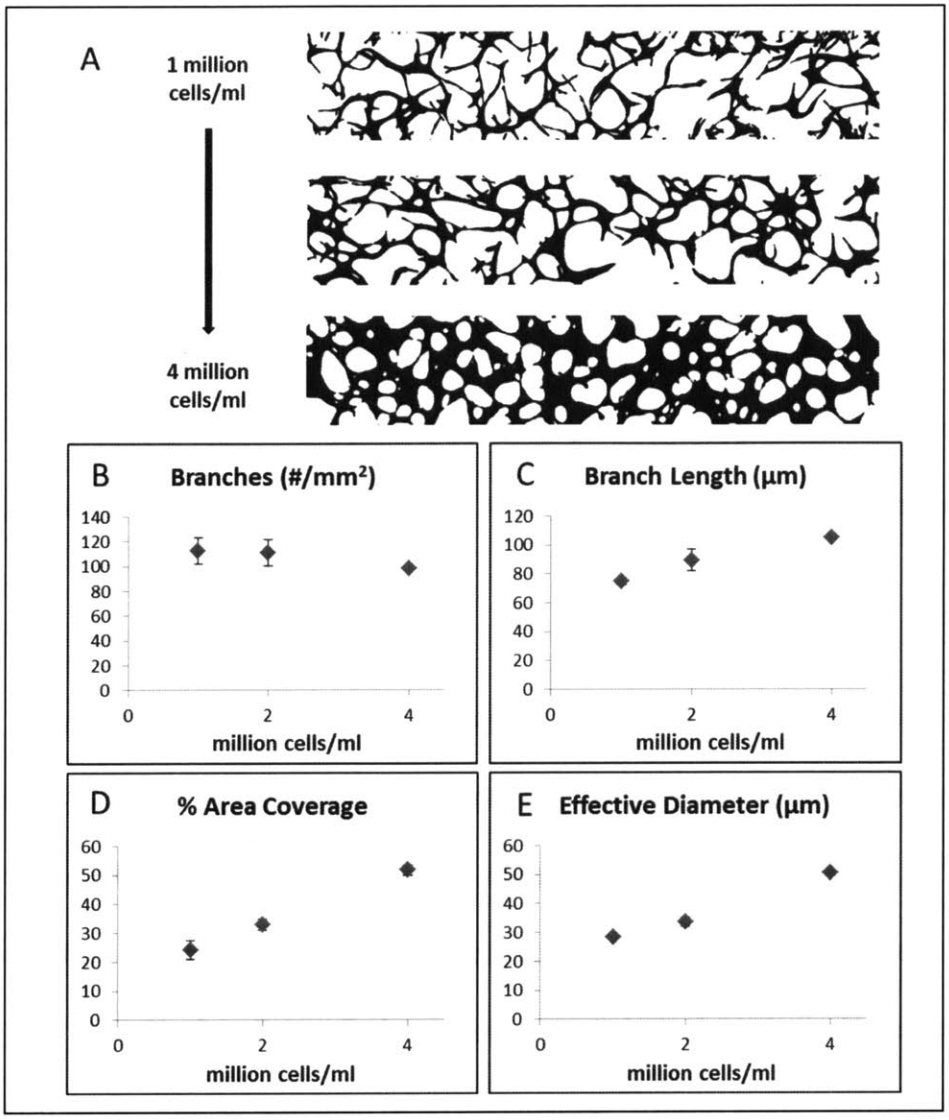

Figure 20. (A) Representative binary images of microvascular networks formed under conditions of increasing HUVEC seeding density. Fixed networks were stained with phalloidin and Imagej was used to process and binarize fluorescent images. (B) Number of branches per mm^2 of vascularized region. Values given are averages over at least 3 devices with error bars given as standard error (same for 4C-E). (C) Average branch length of microvascular network. (D) Percentage of area covered by perfusable microvascular network. (E) Effective diameter of vessels in engineered microvascular network, calculated as the ratio of vascularized area to total length of engineered microvascular network. P-Values given in Appendix II.

Fibroblast Seeding Density

The fibroblasts in our system are physically separated from the HUVECs and their effect on MVN formation is through paracrine signaling. We tested to see whether the amount of

fibroblasts cultured in the stromal cell gel region had a significant impact on the engineered microvascular network morphology. Holding the HUVEC seeding density constant at 4 million cells/ml, we varied the amount of fibroblasts seeded from one half to twice the amount of HUVECs seeded. We found no significant differences in any of the measured microvascular network parameters. Interestingly, we found that the stabilizing effect - as measured by the percentage of perfusable segments at day 6 - was dose dependent on the amount of fibroblasts present and reached a steady maximum value at a HUVEC:HLF ratio of 1:1 (Figure 17C).

Discussion

The ultimate goal of tissue engineering is to replace ailing tissue and failing organs in-vivo. It has been increasingly realized that forming pre-vascularized tissue in-vitro may be a necessary first step.[6,8,56] Additionally, in-vitro platforms enabling the growth and maintenance of a functional microvasculature provide significant benefits in their own right. Perfusable, in-vitro models can be used as physiological drug-screening platforms for developing and identifying metastasis preventing cancer drugs.[57] As demonstrated here, the system can be used to isolate the environmental factors influencing MVN formation and to study their effects. This is an important step in continuing to develop tissue engineering as a quantitative science and to enhance control in the design of tissue engineered constructs.

We successfully formed MVNs using our system containing vessels with diameters ranging between 1-100 μm. These vessels form complex, interconnected networks and are perfusable. It is known that the flow characteristics of blood perfusing through the vasculature is important in determining and maintaining network morphology. In this study, we focused on pre-flow

factors and showed that they direct the early stages of microvascular network formation in vasculogenesis. In future studies, it will be interesting to study the relative importance of flow through the networks after initial formation as it is also likely to play an important role. The presence of chronic shear flow[58] and the introduction of stabilizing pericytes[59,60] would provide a more authentically native microvascular environment and would likely lead to network morphologies that more closely mimic those found in-vivo.

In designing vascularized tissue, it is necessary to consider that, in-vivo, endothelial cells do not form vascular networks in isolation. In addition to mechanical and signaling cues provided by the surrounding extracellular matrix, communication with supporting cell types is critical. Our microfluidic system allows for spatial segregation of various cell types in a compact environment enabling communication through the diffusion of soluble factors.

The stabilizing effect of fibroblasts in our non-contact co-culture system was striking. Without HLFs, the nascent EC networks quickly regressed after initial formation. However, through communication with HLFs, these nascent networks were able to maintain a stable morphology and level of perfusability. It has been shown that fibroblasts enhance MVN formation through direct paracrine signaling[49] and also by adapting the ECM through secreted molecules[50]. It will be interesting in future studies to observe the ECM in real time during MVN formation to characterize this process. It will also be useful to test the effects of various other stromal cells and determine their efficacy in MVN formation for use in regenerative cell therapies.

An important finding from our study is that factors secreted from fibroblasts affect the processes of (a) network formation and (b) stabilization independently. When HUVECs were

cultured with HLFs alone, the networks formed with larger diameter than the control condition and maintained perfusability through day 6. HUVECs cultured with VEGF and S1P formed networks with smaller diameter and regressed with time. Combining HLF co-culture with VEGF and S1P produced networks with smaller diameters that remained stable beyond 1 wk. This suggests that different growth factors might independently control the individual characteristics of network morphology and that this process is also independent of network stabilization. Future work will explore the individual effects of specific growth factors known to be involved in vasculogenesis.

We produced a table of results (Figure 21) which captures our design approach to microvascular engineering and summarizes our findings. In this study, we mapped out the design space for the creation of MVNs with prescribed morphological properties. The controllable inputs we studied were cell seeding densities, ECM composition, and paracrine signaling factors. The output metrics we analyzed were number of branches, average branch length, area fraction of vascularization, and effective diameter. These properties proved sufficient to quantitatively describe the significant differences in network morphology observed by varying environmental conditions.

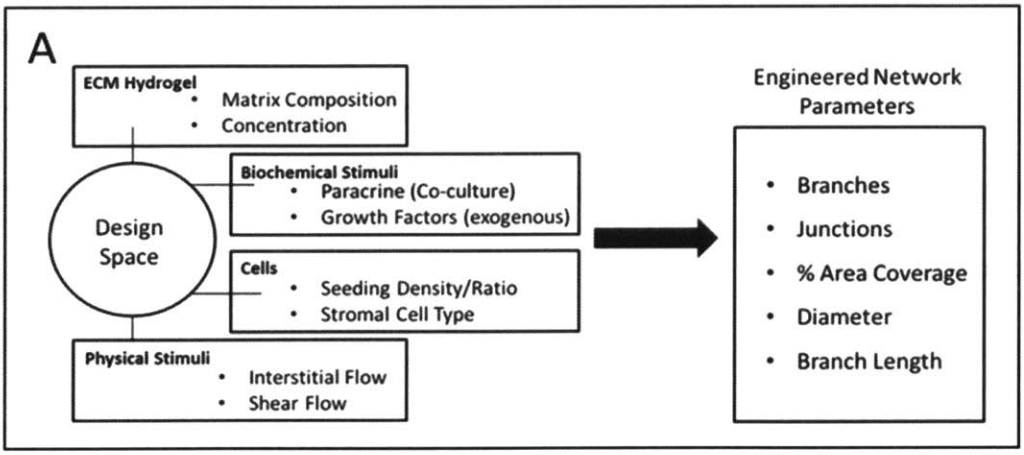

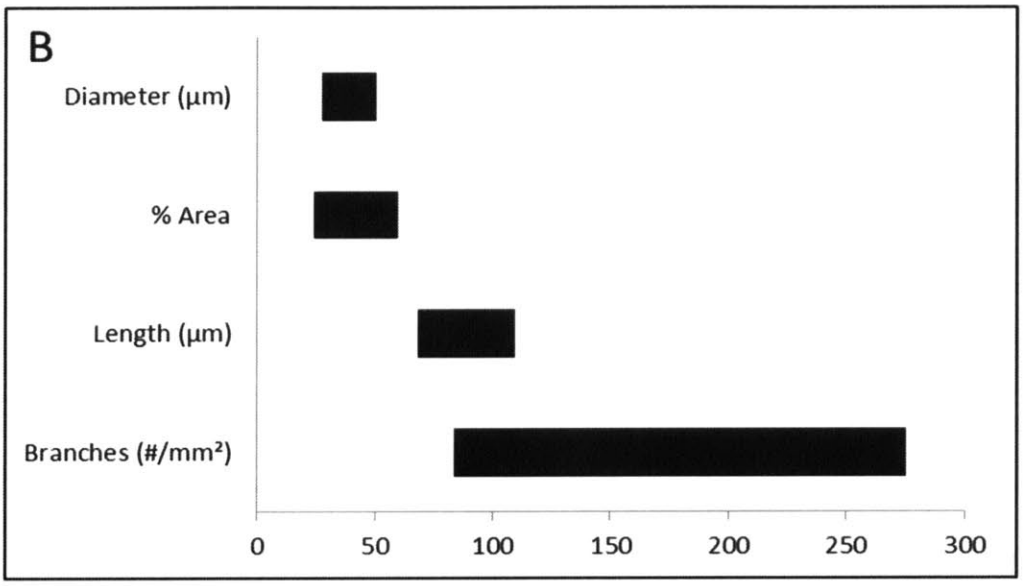

C Condition	Branches	Length	Area	Diameter
VEGF + S1P	↑	↓	↓	↓
Seeding Density (↑)	=	↑	↑	↑
Fibrin Concentration (↑)	↑	↓	=	↓

Figure 21. (A) Diagram of design approach to microvascular tissue engineering. Use of microfluidic platform to quantify effects of mechanical and chemical stimuli on resulting network morphology. Novel, non-contact multi-culture system to study cell-cell communication and network stabilization. (B) Range of network parameters achievable through control of inputs studied. (C) Table of the effects of tunable inputs on distinct network morphological parameters.

The list of environmental factors studied here is not exhaustive, and future work will utilize this system and approach to expand in both breadth and depth. Additionally, to further probe the mechanisms underlying the observations found in this study, it would be useful to pair these

experiments with a computational modeling approach.[61–63] In closing, this study provides a significant contribution to the effort of quantifying the science of microvascular tissue engineering and creating microvascular networks with prescribed morphological properties for tissue specific applications.

Chapter 5: Stem Cells for Microvascular Engineering

Stem cells provide a promising approach to successful tissue engineering and regenerative medicine therapies. The ultimate goal of this strategy is to take a patient's stem cells and differentiate them into the various cell types required to re-grow or repair tissue. This tissue could then be re-introduced into the patient with minimized risk of rejection because the cells are recognized by the host immune system. To this end, we experimented with: 1) human embryonic stem cells (hESC) and 2) mouse embryonic stem cells (mESC).

Human Mesenchymal Stem Cells (hMSCs)

hMSCs can behave as sources for angiogenic paracrine signaling and can also aid in network stabilization by taking on a pericyte phenotype and co-localizing with ECs.[64,65] We studied the potential of hMSCs from human bone marrow to function as such. hMSCs were acquired from the Tulane Center for Gene Therapy and cultured according to the manufacturer's protocol. By seeding ECs and MSCs in opposing medium channels on either side of the gel region, we assessed the angiogenic paracrine signaling potential in non-contact co-culture. To assess the effects of contact co-culture, we seeded ECs and MSCs together; either in the medium channel to replicate sprouting angiogenesis, or together in the gel as in our vasculogenesis model.

We found that non-contact co-culture with MSCs did not induce angiogenic sprouting. Instead, MSCs invaded and populated the gel and sprouting was inhibited. It would be useful to employ one of the methods discussed Chapters 3 and 4 for cell encapsulation in order to inhibit

migration and keep the MSCs isolated from the vascularized region but still able to communicate with the ECs through secretion of soluble factors.

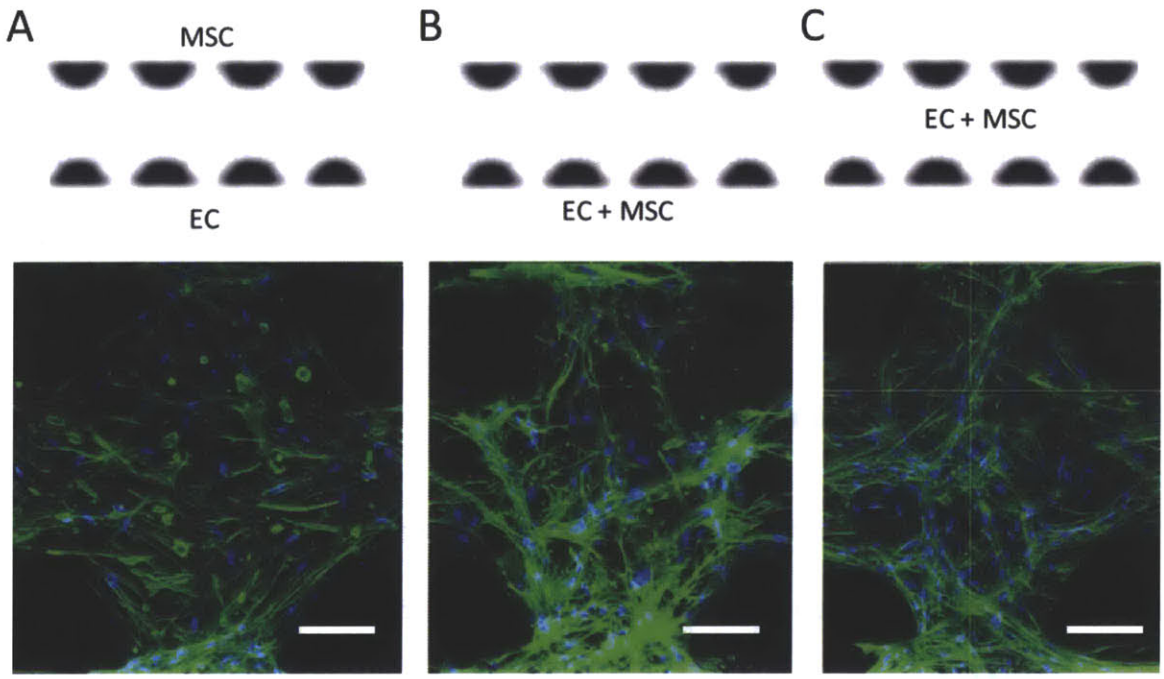

Figure 22. Human bone marrow derived MSCs cultured with ECs in our microfluidic device. Thin, spindle-like cells are MSCs. (A) Non-contact co-culture. MSCs migrate into gel, but EC migration is inhibited. Scale = 100 μm. (B) Contact co-culture in an angiogenesis model. Highly stained regions correspond to endothelial sprouts lined with MSCs. Scale = 100 μm. (C) Contact co-culture in a vasculogenesis model. Scale = 100 μm. Green: phalloidin; Blue: DAPI.

Contact co-culture between ECs and MSCs produced microvascular networks in both angiogenic sprouting and vasculogenesis experiments. Although the MSCs in these experiments also invaded and populated the gel, we did observe dense regions of contact between the two cell types. ECs formed their typical tubular structures and were covered by MSCs. These observations support earlier findings showing the importance of the stage in the process of network formation at which MSCs are introduced.[64]

Mouse Embryonic Stem Cells (mESCs)

In addition to using stem cells as a secondary, supportive cell type, we also explored the potential of using stem cells that have been differentiated towards an EC phenotype in-place of primary ECs. It remains unknown how far along the EC differentiation process stem cells must be brought until they gain vascular network forming functionality. For our experiments, we used Flk1 positive cells derived from embryonic stem cells and further differentiated with VEGF culture. For a detailed protocol, see Glaser et. al., 2011.[66]

We did not observe primary type EC network forming behavior in either of our microfluidic vascularization models. In both angiogenesis and vasculogenesis, mESCs migrated as single cells and failed to form tubular structures or interconnected networks.

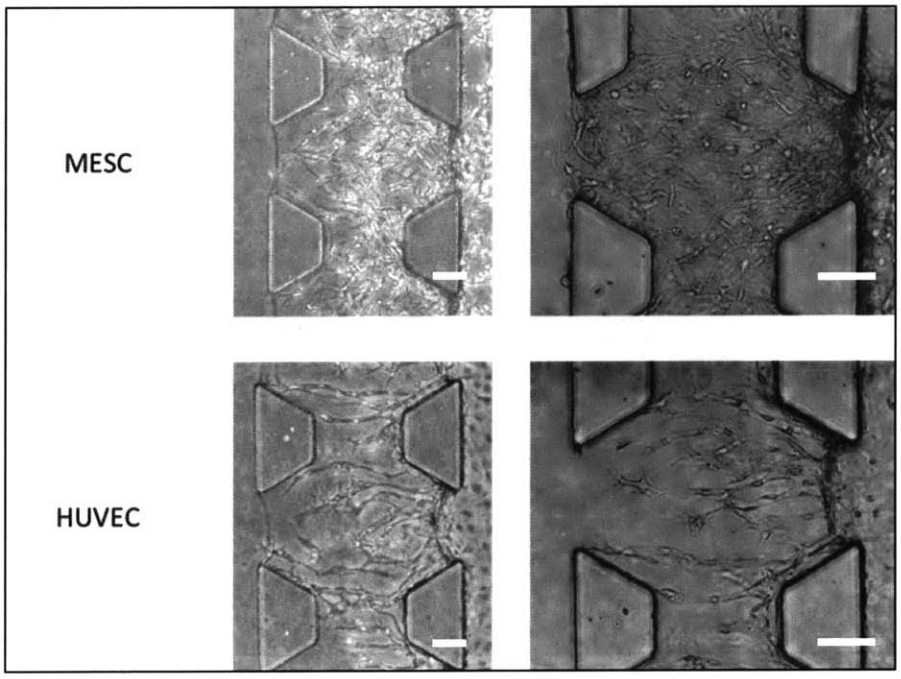

Figure 23. The use of mESCs was explored as a replacement for HUVECs in our sprouting angiogenesis model. Cells migrated as single cells and failed to form multicellular tubular structures. Scale = 100 μm.

It is unclear why the mESCs failed to form vascular networks in our system. It is possible that the cells were never differentiated enough to begin with, or that the population was not sufficiently purified. This would explain why the cells took on a more fibroblast-like and invasive phenotype in our angiogenesis experiments. Since these cells were frozen and thawed, it is possible that the cells de-differentiated and lost their EC specific functionality.

In the vasculogenesis experiments, the mESCs similarly failed to form the vascular networks typical of primary ECs. It would be useful to attempt vascular network formation in our system with human ESCs since they can be stably cultured and might function similarly to HUVECs.[67,68]

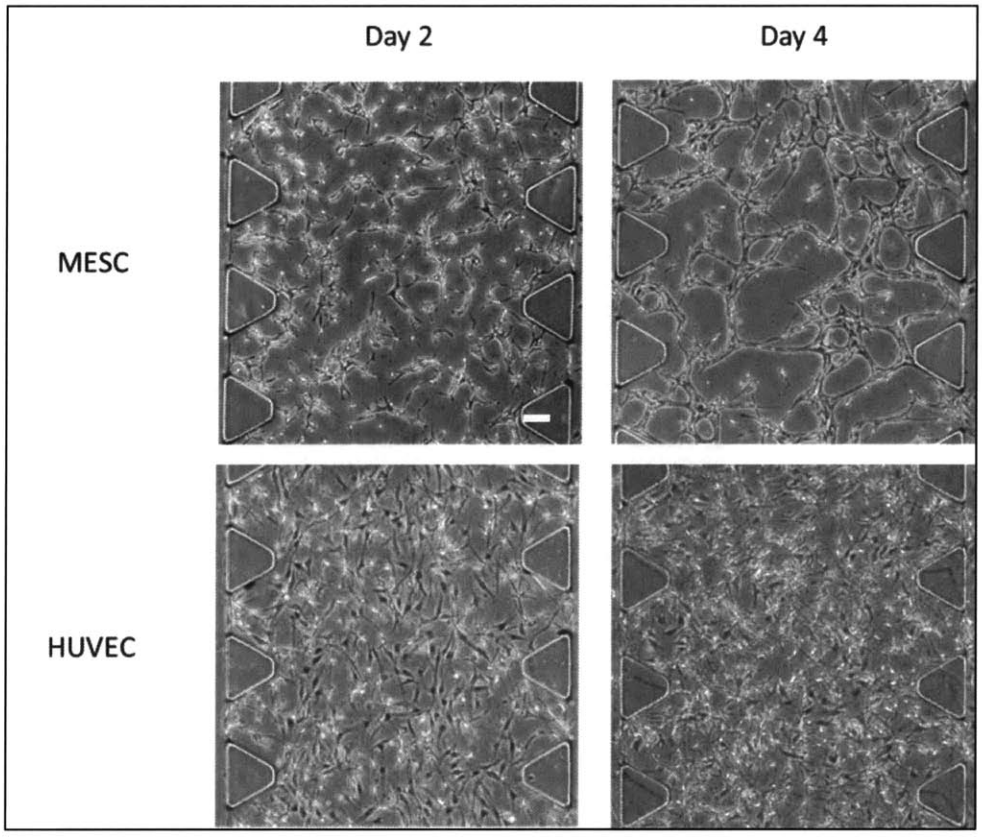

Figure 24. The use of mESCs was explored as a replacement for HUVECs in our sprouting angiogenesis model. mESCs displayed cobblestone morphology when cultured on a 2D surface, as expected of ECs, but failed to form tubular multicellular structures in a 3D hydrogel culture. Scale = 100 µm.

These findings are important in that they suggest that traditional markers used to identify stem cell differentiation into a specific cell type do not necessarily imply that they possess the full functionality of that cell type. Our microfluidic, 3D environment which simulates physiological conditions provides a useful tool in assessing this functionality and the ultimate efficacy of these potentially therapeutic cells.

Conclusion and Future Directions

In this thesis, we developed a reliable platform for engineering perfusable microvascular networks on-demand using state of the art microfluidics technology. We have demonstrated the utility of this platform for studying cancer metastasis and as a test bed for drug discovery and analysis. In parallel, this platform enabled us to study, in a highly controlled environment, the physiologic processes of angiogenesis and vasculogenesis to further elucidate their underlying mechanisms. Coupling these experiments with a multi-scale modeling approach will enable us to further probe the processes of angiogenesis and early stage development from the molecular signaling level up to the level of tissue morphogenesis.

On the level of basic science, we plan to delve further into the effects of both interstitial and shear flow through our engineered microvascular networks; as we well know that these fluid mechanical forces play an important role in vessel stabilization in-vivo.

In terms of practical applications, we plan to incorporate tissue specific cell types to form artificial tissue constructs for implantation. In this regard, our positive results using human stem cells are highly encouraging.

This platform, and the fundamental characteristics of vascularization that we have used it to uncover, represents a valuable contribution to the fields of tissue engineering and regenerative medicine. We are confident that it will be adapted by the scientific community to aid in solving a wide range of health related problems.

References

1. Fountain, H. Surgeons Implant Synthetic Trachea in Baltimore Man. *New York* (2012). at <http://www.nytimes.com/2012/01/13/health/research/surgeons-transplant-synthetic-trachea-in-baltimore-man.html>
2. Cevallos, M. Transplanted trachea, born in lab, is one of several engineered-organ success stories. *Los Angeles* (2011). at <http://articles.latimes.com/2011/jul/08/news/la-heb-trachea-transplant-stem-cell-20110708>
3. Olson, J. L., Atala, A. & Yoo, J. J. Tissue Engineering: Current Strategies and Future Directions. *Chonnam Med. J.* **47,** 1–13 (2011).
4. Jaklenec, A., Stamp, A., Deweerd, E., Sherwin, A. & Langer, R. Progress in the Tissue Engineering and Stem Cell Industry 'Are we there yet?' *Tissue Eng. Part B Rev.* **18,** 155–166 (2012).
5. Horch, R. E., Kopp, J., Kneser, U., Beier, J. & Bach, A. D. Tissue engineering of cultured skin substitutes. *J. Cell. Mol. Med.* **9,** 592–608 (2005).
6. Kaully, T., Kaufman-Francis, K., Lesman, A. & Levenberg, S. Vascularization—The Conduit to Viable Engineered Tissues. *Tissue Eng. Part B Rev.* **15,** 159–169 (2009).
7. Lovett, M., Lee, K., Edwards, A. & Kaplan, D. L. Vascularization strategies for tissue engineering. *Tissue Eng. Part B Rev.* **15,** 353–370 (2009).
8. Gibot, L., Galbraith, T., Huot, J. & Auger, F. A. A preexisting microvascular network benefits in vivo revascularization of a microvascularized tissue-engineered skin substitute. *Tissue Eng. Part A* **16,** 3199–3206 (2010).
9. Levenberg, S. *et al.* Engineering vascularized skeletal muscle tissue. *Nat. Biotechnol.* **23,** 879–884 (2005).
10. Inamdar, N. K. & Borenstein, J. T. Microfluidic cell culture models for tissue engineering. *Curr. Opin. Biotechnol.* **22,** 681–689 (2011).
11. Vickerman, V. & Kamm, R. D. Mechanism of a flow-gated angiogenesis switch: early signaling events at cell–matrix and cell–cell junctions. *Integr. Biol.* **4,** 863 (2012).
12. Sudo, R. *et al.* Transport-mediated angiogenesis in 3D epithelial coculture. *FASEB J.* **23,** 2155–2164 (2009).
13. Wood, L. B., Ge, R., Kamm, R. D. & Asada, H. H. Nascent vessel elongation rate is inversely related to diameter in in vitro angiogenesis. *Integr. Biol.* **4,** 1081–1089 (2012).
14. Shin, Y. *et al.* Microfluidic assay for simultaneous culture of multiple cell types on surfaces or within hydrogels. *Nat. Protoc.* **7,** 1247–1259 (2012).
15. Vickerman, V., Blundo, J., Chung, S. & Kamm, R. Design, fabrication and implementation of a novel multi-parameter control microfluidic platform for three-dimensional cell culture and real-time imaging. *Lab. Chip* **8,** 1468 (2008).
16. Farahat, W. A. *et al.* Ensemble Analysis of Angiogenic Growth in Three-Dimensional Microfluidic Cell Cultures. *PLoS ONE* **7,** e37333 (2012).
17. Neumann, T., Nicholson, B. S. & Sanders, J. E. Tissue engineering of perfused microvessels. *Microvasc. Res.* **66,** 59–67 (2003).
18. Yeon, J. H., Ryu, H. R., Chung, M., Hu, Q. P. & Jeon, N. L. In vitro formation and characterization of a perfusable three-dimensional tubular capillary network in microfluidic devices. *Lab. Chip* **12,** 2815–2822 (2012).
19. Chrobak, K. M., Potter, D. R. & Tien, J. Formation of perfused, functional microvascular tubes in vitro. *Microvasc. Res.* **71,** 185–196 (2006).

20. Chan, E.-S. *et al.* Effect of formulation of alginate beads on their mechanical behavior and stiffness. *Particuology* **9,** 228–234 (2011).
21. Tan, W.-H. & Takeuchi, S. Monodisperse Alginate Hydrogel Microbeads for Cell Encapsulation. *Adv. Mater.* **19,** 2696–2701 (2007).
22. Chan, J. M. *et al.* Engineering of In Vitro 3D Capillary Beds by Self-Directed Angiogenic Sprouting. *PLoS ONE* **7,** e50582 (2012).
23. Kim, C. *et al.* Rapid exchange of oil-phase in microencapsulation chip to enhance cell viability. *Lab. Chip* **9,** 1294–1297 (2009).
24. Chen, M., Whisler, J., Jeon, J. & Kamm, R. Mechanisms of Tumor Cell Extravasation in an In Vitro Microvascular Network Platform. *Submitted*
25. Kassab, G. S. Scaling laws of vascular trees: of form and function. *Am. J. Physiol. Heart Circ. Physiol.* **290,** H894–903 (2006).
26. Hoganson, D. M. *et al.* Principles of Biomimetic Vascular Network Design Applied to a Tissue-Engineered Liver Scaffold. *Tissue Eng. Part A* **16,** 1469–1477 (2010).
27. Murray, C. D. The Physiological Principle of Minimum Work I. The Vascular System and the Cost of Blood Volume. *Proc. Natl. Acad. Sci.* **12,** 207–214 (1926).
28. Barber, R. W. & Emerson, D. R. Biomimetic design of artificial micro-vasculatures for tissue engineering. *Altern. Lab. Anim. ATLA* **38 Suppl 1,** 67–79 (2010).
29. Okkels, F. & Jacobsen, J. C. B. Dynamic adaption of vascular morphology. *Front. Fractal Physiol.* **3,** 390 (2012).
30. Pries, A. R., Secomb, T. W. & Gaehtgens, P. Design Principles of Vascular Beds. *Circ. Res.* **77,** 1017–1023 (1995).
31. Borenstein, J. T. *et al.* Functional endothelialized microvascular networks with circular cross-sections in a tissue culture substrate. *Biomed. Microdevices* **12,** 71–79 (2010).
32. Kim, S., Lee, H., Chung, M. & Jeon, N. L. Engineering of functional, perfusable 3D microvascular networks on a chip. *Lab. Chip* **13,** 1489–1500 (2013).
33. Moya, M. L., Hsu, Y.-H., Lee, A. P., Hughes, C. C. W. & George, S. C. In Vitro Perfused Human Capillary Networks. *Tissue Eng. Part C Methods* 130228102346001 (2013). doi:10.1089/ten.tec.2012.0430
34. Liu, W. *et al.* Fibrin Fibers Have Extraordinary Extensibility and Elasticity. *Science* **313,** 634–634 (2006).
35. Potente, M., Gerhardt, H. & Carmeliet, P. Basic and Therapeutic Aspects of Angiogenesis. *Cell* **146,** 873–887 (2011).
36. Raeber, G. P., Lutolf, M. P. & Hubbell, J. A. Molecularly Engineered PEG Hydrogels: A Novel Model System for Proteolytically Mediated Cell Migration. *Biophys. J.* **89,** 1374–1388 (2005).
37. Yamamura, N., Sudo, R., Ikeda, M. & Tanishita, K. Effects of the Mechanical Properties of Collagen Gel on the In Vitro Formation of Microvessel Networks by Endothelial Cells. *Tissue Eng.* **13,** 1443–1453 (2007).
38. Roeder, B. A., Kokini, K., Sturgis, J. E., Robinson, J. P. & Voytik-Harbin, S. L. Tensile Mechanical Properties of Three-Dimensional Type I Collagen Extracellular Matrices With Varied Microstructure. *J. Biomech. Eng.* **124,** 214–222 (2002).
39. Jain, R. K. Molecular regulation of vessel maturation. *Nat. Med.* **9,** 685–693 (2003).
40. Spiegel, S. & Milstien, S. Sphingosine-1-phosphate: an enigmatic signalling lipid. *Nat. Rev. Mol. Cell Biol.* **4,** 397–407 (2003).
41. Carmeliet, P. & Jain, R. K. Angiogenesis in cancer and other diseases. *Nature* **407,** 249–257 (2000).
42. Polacheck, W. J., Li, R., Uzel, S. G. M. & Kamm, R. D. Microfluidic platforms for mechanobiology. *Lab. Chip* **13,** 2252–2267 (2013).

43. Cunningham, K. S. & Gotlieb, A. I. The role of shear stress in the pathogenesis of atherosclerosis. *Lab. Invest.* **85,** 9–23 (2004).
44. Polacheck, W. J., Charest, J. L. & Kamm, R. D. Interstitial flow influences direction of tumor cell migration through competing mechanisms. *Proc. Natl. Acad. Sci. U. S. A.* **108,** 11115–11120 (2011).
45. Song, J. W. & Munn, L. L. Fluid forces control endothelial sprouting. *Proc. Natl. Acad. Sci.* **108,** 15342–15347 (2011).
46. Chung, S. *et al.* Cell migration into scaffolds under co-culture conditions in a microfluidic platform. *Lab. Chip* **9,** 269–275 (2009).
47. Lim, S. H., Kim, C., Aref, A. R., Kamm, R. D. & Raghunath, M. Complementary effects of prolyl hydroxylase inhibitors and sphingosine 1-phosphate on fibroblasts and endothelial cells in driving capillary sprouting. *Submitted*
48. Arganda-Carreras, I., Fernández-González, R., Muñoz-Barrutia, A. & Ortiz-De-Solorzano, C. 3D reconstruction of histological sections: Application to mammary gland tissue. *Microsc. Res. Tech.* **73,** 1019–1029 (2010).
49. Nakatsu, M. N. *et al.* Angiogenic sprouting and capillary lumen formation modeled by human umbilical vein endothelial cells (HUVEC) in fibrin gels: the role of fibroblasts and Angiopoietin-1☆. *Microvasc. Res.* **66,** 102–112 (2003).
50. Newman, A. C., Nakatsu, M. N., Chou, W., Gershon, P. D. & Hughes, C. C. W. The requirement for fibroblasts in angiogenesis: fibroblast-derived matrix proteins are essential for endothelial cell lumen formation. *Mol. Biol. Cell* **22,** 3791–3800 (2011).
51. Janmey, P. A., Winer, J. P. & Weisel, J. W. Fibrin gels and their clinical and bioengineering applications. *J. R. Soc. Interface* **6,** 1–10 (2009).
52. Piechocka, I. K., Bacabac, R. G., Potters, M., MacKintosh, F. C. & Koenderink, G. H. Structural Hierarchy Governs Fibrin Gel Mechanics. *Biophys. J.* **98,** 2281–2289 (2010).
53. Brown, A. E. X., Litvinov, R. I., Discher, D. E., Purohit, P. K. & Weisel, J. W. Multiscale Mechanics of Fibrin Polymer: Gel Stretching with Protein Unfolding and Loss of Water. *Science* **325,** 741–744 (2009).
54. Ryan, E., Mockros, L., Weisel, J. & Lorand, L. Structural origins of fibrin clot rheology. *Biophys. J.* **77,** 2813–2826 (1999).
55. Ghajar, C. M. *et al.* The Effect of Matrix Density on the Regulation of 3-D Capillary Morphogenesis. *Biophys. J.* **94,** 1930–1941 (2008).
56. Laschke, M. W. *et al.* Angiogenesis in Tissue Engineering: Breathing Life into Constructed Tissue Substitutes. *Tissue Eng.* **12,** 2093–2104 (2006).
57. Ghaemmaghami, A. M., Hancock, M. J., Harrington, H., Kaji, H. & Khademhosseini, A. Biomimetic tissues on a chip for drug discovery. *Drug Discov. Today* **17,** 173–181 (2012).
58. Skalak, T. C. & Price, R. J. The role of mechanical stresses in microvascular remodeling. *Microcirc. New York N 1994* **3,** 143–165 (1996).
59. Von Tell, D., Armulik, A. & Betsholtz, C. Pericytes and vascular stability. *Exp. Cell Res.* **312,** 623–629 (2006).
60. Armulik, A., Abramsson, A. & Betsholtz, C. Endothelial/Pericyte Interactions. *Circ. Res.* **97,** 512–523 (2005).
61. Merks, R. M. H., Brodsky, S. V., Goligorksy, M. S., Newman, S. A. & Glazier, J. A. Cell elongation is key to in silico replication of in vitro vasculogenesis and subsequent remodeling. *Dev. Biol.* **289,** 44–54 (2006).
62. Czirok, A. & Little, C. D. Pattern formation during vasculogenesis. *Birth Defects Res. Part C Embryo Today Rev.* **96,** 153–162 (2012).
63. Merks, R. M. H. & Koolwijk, P. Modeling Morphogenesis in silico and in vitro: Towards Quantitative, Predictive, Cell-based Modeling. *Math. Model. Nat. Phenom.* **4,** 149–171 (2009).

64. Duffy, G. P., Ahsan, T., O'Brien, T., Barry, F. & Nerem, R. M. Bone marrow-derived mesenchymal stem cells promote angiogenic processes in a time- and dose-dependent manner in vitro. *Tissue Eng. Part A* **15,** 2459–2470 (2009).
65. Sorrell, J. M., Baber, M. A. & Caplan, A. I. Influence of Adult Mesenchymal Stem Cells on In Vitro Vascular Formation. *Tissue Eng. Part A* **15,** 1751–1761 (2009).
66. Glaser, D. E. *et al.* Functional Characterization of Embryonic Stem Cell-Derived Endothelial Cells. *J. Vasc. Res.* **48,** 415–428 (2011).
67. James, D. *et al.* Expansion and maintenance of human embryonic stem cell-derived endothelial cells by TGFβ inhibition is Id1 dependent. *Nat. Biotechnol.* **28,** 161–166 (2010).
68. Nourse, M. B. *et al.* VEGF Induces Differentiation of Functional Endothelium From Human Embryonic Stem Cells Implications for Tissue Engineering. *Arterioscler. Thromb. Vasc. Biol.* **30,** 80–89 (2010).

Appendix I: Seeding ECs in Fibrin Gel

Reagents from Sigma:

Fibrinogen
F8630-1G

Thrombin
T4648-1KU

Preparation:

Dissolve thrombin and freeze in 50-100 ul aliquots at 100 U/ml

Dissolve fibrinogen in PBS to 5 mg/ml

- Allow to dissolve for several hours in the water bath, mixing occasionally by hand
- This solution can be kept at 4 degrees, but should be used within 2 weeks

Procedure:

1. Prepare 20 µl aliquots (1 per device to be filled) from 5 mg/ml fibrinogen stock solution in 500 µl Eppindorf tubes and **keep over ice**.
2. Dilute thrombin stock solution in cell medium: 40 µl thrombin solution in 1 ml medium
3. Prepare ECs and re-suspend in the thrombin solution above at 6 million cells per ml: **keep over ice.**
4. Add 20 µl from thrombin/cell suspension into one 500 µl Eppindorf tube containing fibrinogen solution prepared above. Mix gently by pipette aspiration 3-4 times **over ice**.
5. Use P20 pipette to extract 10 µl and fill device
6. Place in humidity box for 5-10 minutes and leave at room temperature
7. Remove from humidity box and fill device with fresh warm medium

Appendix II: P-Values for Figures 17-20

P-values for two-tailed Student's t-distribution. Values correspond to p-values calculated for all combinations of two data points on a given plot. For example, T12 corresponds to the p-value comparing conditions 1 and 2. Values less than 0.05 are in bold.

Figure 17B

	Control	FB
T12	0.4190	**0.0287**
T13	**0.0354**	**0.0118**
T23	**0.0063**	0.7109

Figure 17C

	Control	FB
T12	0.2331	**0.0062**
T13	**0.0291**	**0.0003**
T23	0.1263	0.8194

Figure 17D

T12	**0.0015**
T13	**0.0011**
T14	**0.0000**
T23	0.1416
T24	**0.0289**
T34	0.8157

Figure 18

	Branches	Length	% Area	Diameter
T12	0.1408	0.8727	**0.0021**	**0.0162**
T13	**0.0409**	**0.0091**	**0.0252**	**0.0012**
T14	**0.0000**	**0.0018**	**0.0000**	**0.0030**
T23	0.0832	**0.0016**	**0.0021**	**0.0001**
T24	**0.0000**	**0.0000**	**0.0253**	**0.0001**
T34	**0.0003**	0.1025	**0.0004**	**0.0075**

Figure 19

	Branches	Length	% Area	Diameter
T12	0.3229	**0.0361**	0.9290	0.8614
T13	**0.0416**	0.0573	0.6942	0.3623
T14	**0.0002**	**0.0018**	0.6949	**0.0064**
T23	0.1433	0.8692	0.6779	0.2384
T24	**0.0012**	**0.0323**	0.6359	**0.0023**
T34	**0.0132**	0.0630	0.8990	**0.0222**

Figure 20

	Branches	Length	% Area	Diameter
T12	0.9269	0.1447	**0.0819**	**0.0508**
T13	0.2423	**0.0005**	**0.0019**	**0.0001**
T23	0.2918	0.1222	**0.0031**	**0.0010**